



## 1 **Influence of vegetation on occurrence and time distributions** 2 **of regional new aerosol particle formation and growth**

3 Imre SALMA<sup>1,2</sup>, Wanda THÉN<sup>1,3</sup>, Pasi AALTO<sup>4</sup>, Veli-Matti KERMINEN<sup>4</sup>, Anikó KERN<sup>5</sup>,  
4 Zoltán BARCZA<sup>2,6,7</sup>, Tuukka PETÄJÄ<sup>4</sup>, and Markku KULMALA<sup>4</sup>

5 <sup>1</sup> Institute of Chemistry, Eötvös University, Budapest, Hungary

6 <sup>2</sup> Excellence Center, Faculty of Science, Eötvös University, Martonvásár, Hungary

7 <sup>3</sup> Hevesy György Ph. D. School of Chemistry, Eötvös University, Budapest, Hungary

8 <sup>4</sup> Institute for Atmospheric and Earth System Research, University of Helsinki, Helsinki, Finland

9 <sup>5</sup> Department of Geophysics and Space Science, Eötvös University, Budapest, Hungary

10 <sup>6</sup> Department of Meteorology, Eötvös University, Budapest, Hungary

11 <sup>7</sup> Faculty of Forestry and Wood Sciences, Czech University of Life Sciences, Prague, Czech Republic

12 *Correspondence to:* Imre Salma (salma@chem.elte.hu)

13 **Abstract.** Occurrence frequency ( $f_{\text{NPF}}$ ) of regional atmospheric new aerosol particle formation  
14 (NPF) and consecutive growth events were studied with respect to vegetation activity, aerosol  
15 properties, air pollutants and meteorological data in Budapest over the time interval of 2008–  
16 2018. The data set evaluated contained results of in situ measurements on land surface mostly  
17 performed at the Budapest platform for Aerosol Research and Training Laboratory, of satellite-  
18 based products recorded by MODIS on Terra and of modelled vegetation emission-related  
19 properties from an advanced regional biogeochemical model. Annual mean relative occurrence  
20 frequencies were considerable (with an overall mean of 21 %), remained at a constant level  
21 (with an overall SD of 5 %) and did not exhibit tendentious change over the years. The shape  
22 of the distributions of monthly mean  $f_{\text{NPF}}$  exhibited large variability from year to year, while  
23 the overall distribution already possessed a characteristic pattern. This structure of the NPF  
24 occurrence distributions was compared to those of environmental variables including  
25 concentrations of gas-phase  $\text{H}_2\text{SO}_4$ ,  $\text{SO}_2$ ,  $\text{O}_3$ ,  $\text{NO}$ ,  $\text{NO}_2$ ,  $\text{CO}$ ,  $\text{PM}_{10}$  mass and  $\text{NH}_3$ , of particle  
26 numbers in the size fractions of 6–1000, 6–100 and 100–1000 nm, condensation sink, air  
27 temperature ( $T$ ), relative humidity, wind speed (WS), atmospheric pressure, global solar  
28 radiation, gross primary production of vegetation, leaf area index and stomatal conductance.  
29 There were no evident systematic similarities between  $f_{\text{NPF}}$  on one hand and all variables on  
30 the other hand, except for  $\text{H}_2\text{SO}_4$  and perhaps  $\text{NH}_3$ . The spring maximum in the NPF  
31 occurrence frequency distribution often overlapped with the time intervals of positive  $T$   
32 anomaly on vegetated territories. The link between the potential heat stress exerted on plants  
33 in sultry summer intervals and the summer  $f_{\text{NPF}}$  minimum could not be proved. The relevance  
34 of environmental variables was assessed by their ratios on NPF event day and on non-event  
35 days. Gas-phase  $\text{H}_2\text{SO}_4$  concentration showed the largest monthly ratios, followed by  $\text{O}_3$ . The



36 WS, biogenic precursor gases and SO<sub>2</sub> can generally favour NPF events although their  
37 influence seemed to be constrained. Association between the  $f_{\text{NPF}}$  and vegetation growth  
38 dynamics was clearly identified.

### 39 **1 Introduction and objectives**

40 New aerosol particle formation (NPF) from atmospheric vapours and consecutive particle  
41 diameter growth events (Kulmala et al., 2014) were observed in all major continental  
42 environments in the world (e.g. Kerminen et al., 2018; Nieminen et al., 2018 and references  
43 therein). Their relevance for global aerosol burden, climate system and health risk issues are  
44 increasingly recognised (Spracklen et al., 2006; Makkonen et al., 2009, 2012; Merikanto et al.,  
45 2009; Yue et al., 2010; Sihto et al., 2011; Kerminen et al., 2012; Carslaw et al., 2013; Braakhuis  
46 et al., 2014; Salma et al., 2015; Dunne et al., 2016; Gordon et al., 2016; Ohlwein et al., 2019).  
47

48 Occurrence of NPF events is one of the fundamental properties of the phenomenon. The main  
49 circumstances influencing the regional NPF occurrence involve atmospheric chemical  
50 composition together with concentration and size distribution of aerosol particles,  
51 photochemical processes and meteorological properties (Kulmala et al., 2014). Some precursor  
52 compounds and their oxidation products such as SO<sub>2</sub> and H<sub>2</sub>SO<sub>4</sub>, volatile organic compounds  
53 (VOCs) and extremely low volatility organic compounds (ELVOCs) or highly oxygenated  
54 molecules (HOMs), NH<sub>3</sub> or amines, iodine oxides and HIO<sub>3</sub> were shown to influence NPF  
55 events (O'Dowd et al., 2002; Sipilä et al., 2010, 2016; Metzger et al., 2010; Kirkby et al., 2011,  
56 2016; Riipinen et al., 2011; Almeida et al., 2013; Donahue et al., 2013; Schobesberger et al.,  
57 2013; Ehn et al., 2014; Riccobono et al., 2014; Jokinen et al., 2015; Bianchi et al., 2016; Tröstl  
58 et al., 2016; Yao et al., 2018; Kürten, 2019; He et al., 2020). Further chemical species such as  
59 isoprene or NO<sub>2</sub> showed inhibiting effects (Kiendler-Scharr et al., 2009; Lehtipalo et al., 2016;  
60 Heinritzi et al., 2020; Simon et al., 2020). It was pointed out that NPF can proceed from HOMs  
61 alone when it is assisted by air ions (Kirkby et al., 2016). These conclusions were derived  
62 mostly from environmental or plant atmosphere chamber experiments. Meteorological  
63 parameters such as solar radiation, air temperature ( $T$ ), water vapour content or relative  
64 humidity (RH), wind speed (WS), boundary mixing layer height can also favour or depress  
65 NPF events (Birmili and Wiedensohler 2000; Hamed et al., 2011; Hirsikko et al., 2012; Jun et  
66 al., 2014; Dada et al., 2017). The actual occurrence may also be associated with some limiting  
67 or triggering atmospheric processes in the region (Manninen et al., 2010; Dall'Osto et al., 2013).



68 Galactic cosmic rays do not seem to contribute extensively to the overall nucleation under  
69 ordinary environmental conditions (e.g. in the presence of atmospheric chemical bases or  
70 HOMs) and particularly in the lower troposphere (Kirkby et al., 2011; 2016; Almeida et al.,  
71 2013; Riccobono et al., 2014; Dunne et al., 2016). As a consequence of all these factors, NPF  
72 events happen with a varying frequency in space and time.

73

74 The annual relative occurrence frequency of NPF events is typically between 10 % and 40 %  
75 for many geographical regions (Brines et al., 2015; Xiao et al., 2015; Kerminen et al., 2018;  
76 Nieminen et al., 2018; Bousiotis et al., 2019; Lee et al., 2019). The frequency changes  
77 substantially over a year since most multifactorial conditions and the complex interplay among  
78 the environmental variables influencing it have prominent seasonal variation (Tunved et al.,  
79 2006). Many studies reported spring or summer maximum (Qian et al., 2007; Wu et al., 2007;  
80 Meija and Morawska, 2009; Manninen et al., 2010; Salma et al., 2011; Vakkari et al., 2011;  
81 Hirsikko et al., 2012; Nieminen et al., 2014; Dall'Osto et al., 2018). This is, however, not  
82 universal, and the order of the seasons can vary among individual territories. Reliable  
83 experimental determination of the annual and monthly mean frequencies of regional NPF  
84 require several-year-long semi-continuous measurements since the occurrence can be  
85 influenced by inter-annual differences in chemical, aerosol and meteorological properties and  
86 in biogenic cycling.

87

88 It was also attempted to predict the distributions of the monthly mean occurrence frequency by  
89 combining the effects of environmental variables which can be derived from routine  
90 atmospheric measurements (e.g. Clement et al., 2001; Boy and Kulmala, 2002; Mikkonen et  
91 al., 2006). Conclusive prognostic or explanative methods could not be, however, achieved  
92 (Kerminen et al., 2018). This also means that the driving factors of NPF occurrence and their  
93 time variation have remained largely unidentified, poorly understood and unexplained. The  
94 lack of this knowledge and experimental information also hinders our understanding the role  
95 of anthropogenic activities in related societal issues of aerosol particles such as their climate  
96 and health effects.

97

98 Several-year-long, semi-continuous, critically evaluated and complex atmospheric data sets are  
99 available for the Budapest area. The major objectives of this study are 1) to determine and  
100 discuss the annual mean relative occurrence frequency and the distributions of monthly mean  
101 frequency of NPF events in Budapest for seven full measurement years in 2008–2018, 2) to



102 investigate and explain the changes in the shape of the distributions and their annual mean with  
103 respect to basic meteorological data, criteria air pollutants and other environmental factors  
104 including vegetation-related variables and 3) to evaluate and interpret the effects of vegetation  
105 on NPF occurrence together with the incidence between them. The involvement of the  
106 vegetation-related factors into the ambient NPF and their combination with the environmental  
107 influencing properties represent a noteworthy novelty in the research field. The present survey  
108 also prepares the full exploitation of the data base by advanced multi-variate statistical  
109 methods.

## 110 **2 Data sets**

111 The following environmental variables were considered in the study: number of NPF event  
112 days and non-event days, particle number concentrations in the diameter ranges from 6 to 1000  
113 nm ( $N$ ), from 6 to 100 nm ( $N_{6-100}$ ) and from 100 to 1000 nm ( $N_{100-1000}$ ), concentrations of gas-  
114 phase  $\text{H}_2\text{SO}_4$ ,  $\text{SO}_2$ ,  $\text{O}_3$ ,  $\text{NO}$ ,  $\text{NO}_x$ ,  $\text{NO}_2$ ,  $\text{CO}$ ,  $\text{PM}_{10}$  mass and  $\text{NH}_3$ , condensation sink (CS),  $T$ ,  
115 RH, WS, atmospheric pressure ( $P$ ), global solar radiation (GRad), gross primary production  
116 (GPP) of vegetation, leaf area index (LAI), stomatal conductance (SCT) and characteristics of  
117 vegetation growth dynamics such as start of spring (SoS) and green-up duration (GuD). Most  
118 variables were determined experimentally, while the variables (last five properties) related to  
119 vegetation were derived from an advanced regional biogeochemical model or from satellite-  
120 based vegetation products. The data sets actually evaluated in comparisons contained daily  
121 median atmospheric concentrations, daily means and standard deviations (SDs) for all variables  
122 and daily maximum values for GRad ( $\text{GRad}_{\max}$ ). The individual data were averaged over each  
123 month, then separately for NPF event days and non-event day in each month, and finally over  
124 all measurement years in the city centre.

125

126 The time intervals investigated comprise seven full measurement years, i.e. Y1) from 3  
127 November 2008 to 2 November 2009, Y2) from 19 January 2012 to 18 January 2013, Y3) from  
128 13 November 2013 to 12 November 2014, Y4) from 13 November 2014 to 12 November 2015,  
129 Y5) from 13 November 2015 to 12 November 2016, Y6) from 28 January 2017 to 27 January  
130 2018 and Y7) from 28 January 2018 to 27 January 2019. In Sect. 3.5, we also included the NPF  
131 occurrence data for the last full measurement year completed, i.e. from 28 January 2019 to 27  
132 January 2020 (Y8). Our specific purpose by adding this year was to improve the statistics in  
133 studying the effect of vegetation on NPF events. Local time ( $\text{LT}=\text{UTC}+1$  or daylight-saving



134 time, UTC+2) was chosen as the time base of the data because it had been observed that the  
135 daily activity time pattern of inhabitants largely influences many atmospheric processes in  
136 cities (Salma et al., 2014; Sun et al., 2019; Mikkonen et al., 2020).

## 137 **2.1 Experimental data and their treatment**

138 The concentrations  $N$ ,  $N_{6-100}$  and  $N_{100-1000}$  were determined by a flow-switching type  
139 differential mobility particle sizer (DMPS; Salma et al., 2011, 2016b). Its main components  
140 include a radioactive ( $^{60}\text{Ni}$ ) bipolar charger, a Nafion semi-permeable membrane dryer, a 28-  
141 cm long Vienna-type differential mobility analyser and a condensation particle counter (TSI,  
142 model CPC3775). The measurements were performed in a diameter range from 6 to 1000 nm  
143 in the dry state of particles. The system was updated twice during the years, in spring 2013 and  
144 winter 2016. The major parts of the DMPS system were cleaned and serviced but remained  
145 unchanged. Extensive data validation, calibration or comparative exercises were realised in  
146 summer 2015 and in autumn 2019, which yielded acceptable results (Salma et al., 2016a;  
147 Mikkonen et al., 2020).

148

149 The DMPS data were used for identification and classification of the regional NPF events using  
150 daily particle number size distribution surface plots (Dal Maso et al., 2005; refined by Kulmala  
151 et al., 2012; Németh et al., 2018). The following main classes were separated: event days, non-  
152 event days, undefined days and days with missing data (for more than 4 h during the midday).  
153 Relative occurrence frequency of NPF events ( $f_{\text{NPF}}$ ) was determined for each month and year  
154 as the ratio of the number of event days to the total number of relevant days within the time  
155 interval dealt with. In order to evaluate the timing relationships between vegetation growth and  
156 NPF events (Sect. 3.5), the start of the NPF occurrence peak in spring (see later Fig. 2) had to  
157 be further refined. This was achieved by considering weekly time scale for determining the  
158 occurrence frequency. These data, however, showed larger scatter mainly due to the discrete  
159 daily character of NPF events. Therefore, the weekly occurrence frequency data sets for winter  
160 and spring were subjected to 1-month smoothing to derive less fluctuating time trends. The  
161 start of the NPF occurrence spring peak was set at the date (day of year) of the 20 %-value of  
162 the difference between the maximum smoothed spring peak frequency and the mean winter  
163 level of weekly frequencies (on the early side of the peak).

164

165 The DMPS measurements took place at two urban locations in Budapest, Hungary (Fig. 1). In  
166 the measurement year 2012–2013, they were performed in the near-city background, while in



167 all other years, they were accomplished in the city centre. The former location is situated at the  
168 NW border of Budapest in a wooded area of the Konkoly Astronomical Observatory (N 47°  
169 30' 00", E 18° 57' 47", 478 m above mean sea level, a.m.s.l.) of the Hungarian Academy of  
170 Sciences. This site characterises the air masses which enter the city since the prevailing wind  
171 direction in the area is NW. The measurements in the city centre were conducted at the  
172 Budapest platform for Aerosol Research and Training (BpART) Laboratory (N 47° 28' 30", E  
173 19° 3' 45", 115 m a.m.s.l.) of the Eötvös University (Salma et al., 2016a). It represents a well-  
174 mixed average atmospheric environment for the overall city centre.

175

176

177

178

179

180

181

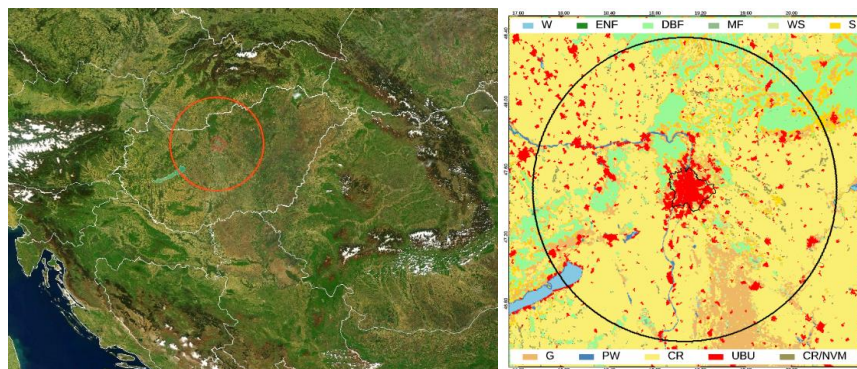
182

183

184

185

186



187

188

189

190

191

192

193

194

195

196

197

198

199

200

201

**Figure 1.** Location of Budapest in the Carpathian Basin and the circular geographical area with a radius of 100 km around it, which was considered in modelling calculations (left), and the spatial distribution of land cover types in IGBP classification (right). Both pictures were derived from satellite-based imagery data recorded by MODIS. W: water bodies, ENF: evergreen needleleaf forests, DBF: deciduous broadleaf forests, MF: mixed forests, WS: woody savannas, S: savannas, G: grasslands, PW: permanent wetlands, CR: croplands, UBU: urban and built-up lands, CR/NVM: cropland and natural vegetation mosaics.

The concentrations of SO<sub>2</sub>, O<sub>3</sub>, NO/NO<sub>x</sub>/NO<sub>2</sub>, CO and PM<sub>10</sub> mass were measured by UV fluorescence (Ysselbach 43C), UV absorption (Ysselbach 49C), chemiluminescence (Thermo 42C), IR absorption (Thermo 48i) and beta-ray attenuation (Thermo FH62-I-R) methods, respectively with a time resolution of 1 h. The data were acquired from the closest measurement station of the National Air Quality Network in Budapest located in 4.5 km from the urban site, and of 6.9 km from the near-city background site in the upwind prevailing direction (Salma and Németh, 2019).



202 It was previously shown that the NPF events observed in the Budapest ordinarily happen above  
203 a larger territory in the Carpathian Basin (Németh and Salma, 2014) as a spatially coherent  
204 regional atmospheric phenomenon (Salma et al., 2016b). Local urban NPF events are  
205 superimposed on regional events in several occasions, which result in growth curves with  
206 multiple or broad onsets. In these cases, the regional events were included in the evaluations.  
207 Considering that NPF events in the Carpathian Basin ordinarily extend over larger horizontal  
208 scales, long-term concentrations of  $\text{NH}_3$ , which are available for the K-pusztá measurement  
209 station, were also accepted in the study. This station (N 46° 57' 56", E 19° 32' 42", 125 m  
210 a.m.s.l.) is situated on the Great Hungarian Plain in a distance of 68 km from the BpART  
211 Laboratory, and it is part of the European monitoring and evaluation of the long-range  
212 transmission of air pollutants (EMEP) network. The  $\text{NH}_3$  concentrations were measured in  
213 daily air samples collected by filter pack method on citric acid-impregnated cellulose filter by  
214 UV-Vis spectrophotometry according to the EMEP protocol (EMEP Manual, 2002; Horváth et  
215 al., 2009).

216

217 Most meteorological measurements for the city centre took place on site at a regular station of  
218 the Hungarian Meteorological Service (HMS, station no. 12843) in approximately 70 m from  
219 the BpART Laboratory. The data of  $T$ , RH, WS and  $P$  were obtained by standardised  
220 meteorological methods (Vaisala HMP45D temperature and humidity probe, Vaisala  
221 WAV15A anemometer and Vaisala PTB210 digital barometer, respectively, all Finland) with  
222 a time resolution of 10 min (except for Y1, when it was 1 h). The WS was measured above the  
223 rooftop level. The basic meteorological data for the near-city background were derived by a  
224 mobile meteorological station installed at the measurement location at a height of ca. 2 m from  
225 the ground with a time resolution of 10 min. Global solar radiation was measured by the HMS  
226 (station no. 44527; CMP11 pyranometer, Kipp and Zonnen, The Netherlands) situated in 10  
227 km in E direction with a time resolution of 1 h. Since 2018, the GRad has been also measured  
228 on site by the BpART Laboratory on the rooftop of the building complex using an SMP3  
229 pyranometer (Kipp and Zonnen, the Netherlands) with a time resolution of 1 min. The annual  
230 mean GRad ratio and SD for 1-h mean values at the BpART Laboratory and HMS station in  
231 2018 were  $1.03 \pm 0.23$  for  $\text{GRad} > 100 \text{ W m}^{-2}$ .

232

233 The Open Database for Climate Change Related Impact Studies in Central Europe (FORESEE,  
234 v. 3.1; Dobor et al., 2014) was utilized to estimate the daily maximum  $T$  data for vegetated  
235 territories within the modelled area (Fig. 1) to study the effect of  $T$  on biogenic emissions. The



236 updated data base (<http://nimbus.elte.hu/FORESEE/>) contains observation-based spatially  
237 interpolated daily meteorological fields on a regular grid with a spatial resolution of  $1/6^{\circ} \times 1/6^{\circ}$   
238 for the interval of 1951–2019 using the E-OBS 17e dataset (Comes et al., 2018). From the daily  
239  $T$  data 8-day means were calculated at the pixel level on the finer grid of the MODIS products  
240 using elevation as supplementary data (Kern et al., 2016). From these  $T$  data, area mean values  
241 were calculated for those pixels which represent vegetated territories (Sect. 2.2.2). Finally, the  
242 difference of the daily maximum  $T$  values from its related multi-annual mean in its  
243 corresponding 8-day time interval were determined as anomaly in maximum air temperature.  
244 In order to assist the later comparison of this differential effect with that of other environmental  
245 properties, the  $T$  anomaly was divided by the SD of the overall mean maximum air temperature  
246 (thus, it was expressed in units of SD). The quantity is referred as standardised  $T$  anomaly.  
247 Standardised NPF occurrence frequency anomaly –used in Sect. 3.3 – was calculated in an  
248 analogous manner to  $T$ .

## 249 2.2 Modelled data

250 Condensation sink for vapour molecules (represented by  $\text{H}_2\text{SO}_4$ ) onto the surface of existing  
251 aerosol particles was computed for discrete size distributions (Kulmala et al., 2013; Dal Maso  
252 et al., 2002, 2005) by computation scripts developed at the University of Helsinki. Dry particle  
253 diameters were considered in the calculations. One of the key components in NPF process is  
254 the gas-phase  $\text{H}_2\text{SO}_4$  (Sihto et al., 2006; Sipilä et al., 2010; Erupe et al., 2011; Lehtipalo et al.,  
255 2018). Its long-term atmospheric measurements are challenging and, therefore, rare. The  
256  $\text{H}_2\text{SO}_4$  concentrations were determined utilising a recently improved calculation method of  
257 Dada et al. (2020) by adopting the fitted coefficients for Budapest and for radiation intensities  
258  $>50 \text{ W m}^{-2}$ . The  $[\text{H}_2\text{SO}_4]$  data obtained were also compared to its proxy derived as  
259  $[\text{SO}_2] \times \text{GRad}/\text{CS}$  (Petäjä et al. 2009), which was used previously for many years. There was  
260 reasonable agreement between their relative changes, e.g. with an overall Pearson's coefficient  
261 of correlation of  $R=0.85$ .

### 262 2.2.1 Vegetation properties related to emissions

263 In order to evaluate the impact of biogenic VOC (BVOC) sources on NPF event occurrence,  
264 three compound vegetation properties, i.e. GPP, LAI and SCT were derived. These three  
265 parameters may be indirectly associated with vegetation emissions and finally with BVOC  
266 concentrations. They were computed by the Biome-BGCMuSo biogeochemical model (v6;  
267 Thornton and Rosenbloom, 2005; Hidy et al., 2016). This is a widely used, process-based





268 model with multilayer soil module that simulates the storage and flux of H<sub>2</sub>O, C and N between  
269 terrestrial managed agro-ecosystems and the atmosphere. The system is driven by daily  
270 meteorological data, eco-physiological properties, soil parameters and some optional input data  
271 such as CO<sub>2</sub> concentration and some site-specific management information to simulate the  
272 biogeochemical processes of a biome. It also accounts for fertilization, harvest and crop  
273 rotation. The system utilised here was parameterized specifically to the Carpathian Basin, and  
274 its proper functioning and outputs were validated by agricultural-related data products and  
275 eddy-covariance measurements (Barcza et al., 2010; Hidy et al., 2016).

276

277 Primary production of the vegetation on land depends on many factors, principally on local  
278 hydrology, soil fertility, plant species composition, photosynthetically active radiation and  
279 disturbance. It is often thought to be proportional to general biogenic activity which involves  
280 BVOC emissions as well. In Biome-BGCMuSo the GPP was calculated using Farquhar's  
281 photosynthesis routine (Farquhar et al., 1980). The LAI is a measure for the total area of leaves  
282 per unit ground area and is directly related to the amount of light that is intercepted by plants.  
283 Virtually, it is considered as a driving parameter for biosphere-atmosphere exchange of CO<sub>2</sub>  
284 and water vapour (Bonan, 2015). The SCT is a measure of the transport rate of H<sub>2</sub>O vapour  
285 exiting through the stomata of leaves, and it also controls parallel assimilation of CO<sub>2</sub>. It is a  
286 function of the density, aperture and size of stomata, and is also related to the boundary layer  
287 resistance of the leaf and the concentration gradient of H<sub>2</sub>O vapour between the leaf and the  
288 atmosphere. Light is the primary stimulus engaged in this process, the second key factor is the  
289 photosynthesis, while plants themselves can also regulate their transpiration rate via their SCT.  
290 Other (organic) gases from plants are also emitted through stomata, and, therefore, the SCT  
291 can also be related to the fluxes of BVOCs from vegetation to the atmosphere. The three  
292 vegetation-related variables were derived in model calculations for a circular geographical area  
293 around Budapest with a radius of 100 km (Fig. 1). Biome-BGCMuSo was run with generic  
294 maize, winter wheat, grassland and broadleaf forest parameterization representing the main  
295 plant functional types (PFT) in the region. The model results were aggregated according to the  
296 share of PFT within the given pixel area.

### 297 **2.2.2 Vegetation growth dynamics**

298 Two phenological indices which are related to vegetation growth dynamics in springtime were  
299 estimated. They are the SoS, which is the onset of vegetation growth after the winter dormancy  
300 and the GuD, which expresses the time period of initial leaf development after SoS. Their



301 determination was accomplished by utilizing the satellite-based, Normalized Difference  
302 Vegetation Index (NDVI) data sets. The NDVI data are graphical indicators of the greenness  
303 of the biomes. They were derived from the latest version (C006) of the official MOD09A1  
304 atmospherically corrected surface reflectance product (Vermote, 2015). This was generated  
305 from the measurements of the MODerate resolution Imaging Spectroradiometer (MODIS)  
306 operating on board of the satellite EOS AM1, Terra (Justice et al., 1998). The data were  
307 downloaded for the h19v04 sinusoidal tile with a spatial resolution of 500 m and a temporal  
308 resolution of 8 d (LP DAAC, 2019) in hierarchical data format for the interval of 2009–2019.

309

310 The land cover data sets for a circular area with a radius of 100 km around Budapest were  
311 derived from the official MCD12Q1 land cover product (Sulla-Menashe and Friedl, 2018) with  
312 a spatial resolution of 500 m for years 2001–2018 according to the International Geosphere  
313 Biosphere Programme (IGBP) classification scheme (Fig. 1). In the modelling, the following  
314 vegetation types were studied: 1) croplands (58 % of all, 117817 pixels), 2) grasslands (13 %),  
315 3) deciduous broadleaf, mixed and evergreen needleleaf forests (12 %; of them, 98 % deciduous  
316 trees) and 4) all vegetation, i.e. all territory types except for urban and built-up lands (6 %),  
317 water bodies (0.9 %) and permanent wetlands (0.6 %).

318

319 Daily-resolution data set was calculated after quality filtering and pre-processing, and then the  
320 characteristics of the spring development were assessed by the methodology of Kern et al.  
321 (2020). From remote-sensing point of view, the green-up dynamics is characterized by a sharp,  
322 mostly linear rise in the NDVI curve that represents leaf flushing (Seyednasrollah et al., 2018),  
323 and which can be characterized by the date of leaf unfolding (as the SoS). The GuD is the time  
324 difference between the date of the end of greening (EoG) and of the SoS. To achieve this, the  
325 NDVI span was calculated as the difference between the maximum and the minimum NDVI  
326 during spring green-up. The SoS and the EoG were set at the date (day of year) when NDVI  
327 reached the lower and upper 20 % of the NDVI span, respectively (e.g. Shen et al., 2015). Both  
328 the SoS and GuD data were determined at the pixel level for each year. Their SDs were also  
329 calculated as characteristics of the spatial variability of the derived metrics. The vegetation  
330 growth for all years and the methodological procedure are summarized in Fig. S1 in the  
331 Supplement. The data sets were processed using the Interactive Data Language (v. 8.6, Harris  
332 Geospatial Solutions, USA).



### 333 3 Results and discussion

334 Annual averages of the environmental variables over most measurement years were already  
335 summarized in accompanying publications (Salma and Németh, 2019; Mikkonen et al., 2020),  
336 and, therefore, the new quantities studied are only overviewed in Table 1. The data are in line with  
337 or comparable to the values ordinarily obtained for the area (Barcza et al., 2010; Salma et al.,  
338 2016b).

339

340 **Table 1.** Number of NPF event days ( $n_{\text{NPF}}$ ), annual median gas-phase  $\text{H}_2\text{SO}_4$  concentration and  $\text{NH}_3$  mixing ratio,  
341 gross primary production (GPP) of vegetation, leaf area index (LAI) and stomatal conductance (SCT) for the  
342 seven measurement years. The measurement unit are indicated in brackets.

343

Measurement year/ Variable	2008– 2009	2012– 2013	2013– 2014	2014– 2015	2015– 2016	2017– 2018	2018– 2019
$n_{\text{NPF}}$	83	96	72	81	35	83	64
$[\text{H}_2\text{SO}_4]$ ( $\times 10^5 \text{ cm}^{-3}$ )	8.8	14.5	8.4	8.7	11.5	10.0	10.4
$[\text{NH}_3]$ (ppb)	2.1	2.0	2.8	2.3	2.5	2.6	3.1
GPP ( $\text{gC m}^{-2} \text{ d}^{-1}$ )	2.5	2.6	3.0	2.7	3.1	2.8	2.9
LAI (%)	71	73	81	82	86	93	70
SCT ( $\times 10^{-3} \text{ m s}^{-1}$ )	1.68	1.62	2.1	1.73	2.1	1.90	1.75

344

345 During the seven measurement years, the total number of NPF events was 514. The annual  
346 means of the relative NPF event occurrence frequency are considerable. The overall six-year  
347 mean and SD for the city centre were  $(21 \pm 5) \%$ . The  $f_{\text{NPF}}$  in year 2015–2016 was unusually low  
348 (its value was ca. 13 %, thus lower by 35 % relatively than the overall mean), but there is no  
349 plausible explanation for this extreme in the present annual data set. The overall mean  
350 frequency and its SD imply that the annual  $f_{\text{NPF}}$  did not change substantially and, more  
351 importantly, in a tendentious manner over the decennial interval studied. It is added as  
352 background information that 1) there was also no significant decreasing trend in major  
353 precursors or interacting gaseous chemical species such as  $\text{SO}_2$  or  $\text{NO}_2$  in the area over the time  
354 interval of interest (Mikkonen et al., 2020, see also Figs. S2 and S6, respectively) and 2) the  
355 overall annual median formation rate of particles with a diameter of 6 nm was  $4.6 \text{ cm}^{-3} \text{ s}^{-1}$ , the  
356 median growth rate for 10-nm particles was  $7.3 \text{ nm h}^{-1}$  over the years studied, and they were  
357 without larger fluctuations and showed summer maximum (Salma and Németh, 2019).



### 3.1 Distributions of NPF event occurrence

Distributions of the monthly mean occurrence frequency of event days for each measurement year are shown in Fig. 2. There are obvious similarities and differences among the distributions. The largest diversity was realised in the measurement year 2015–2016 (that also exhibited the smallest annual mean  $f_{\text{NPF}}$ ). Its shape was flattened and featureless. All the other distributions were much closer to each other in many respects.

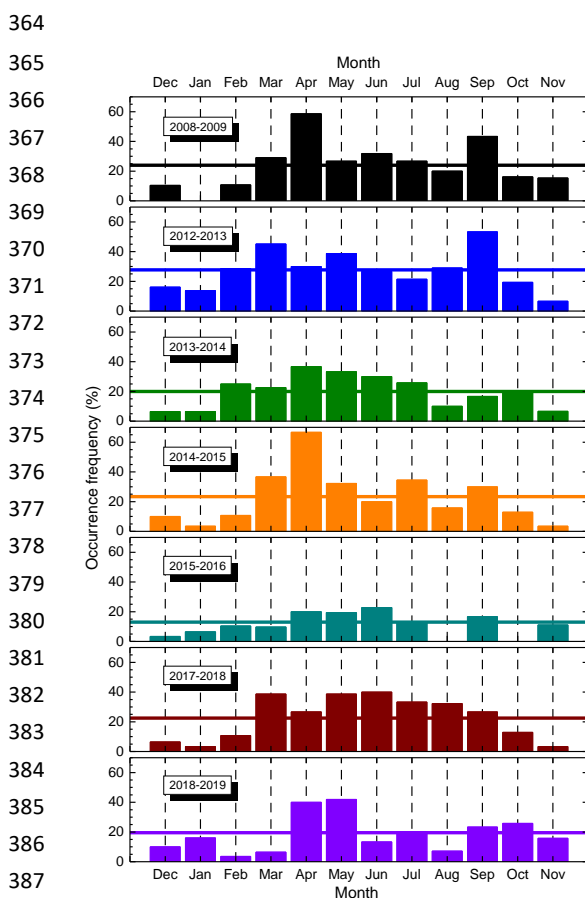


**Figure 2.** Distributions of monthly mean relative occurrence frequency of NPF event days for the seven measurement years. The horizontal lines indicate annual means. The value for January 2009 is zero, while the values for August and October 2016 are not available. The measurements in 2012–2013 were performed in the near-city background, while in the other years, they were accomplished in the city centre.

392

The shapes of the individual distributions also intimated some resemblant components that were repeated over the years. They became more obvious when the overall mean distribution was derived by averaging for all years in the city centre (Fig. 3). The overall distribution



396 exhibits an evident structure which consists of an absolute and a local maximum in April with  
397 a monthly mean occurrence frequency of  $(41\pm 18)$  % and in September with a mean of  
398  $(28\pm 10)$  %, respectively and an absolute and a local minimum in January with a mean of  
399  $(5.9\pm 5.5)$  % and in August with a mean of  $(19.5\pm 9.4)$  %, respectively. The relatively large  
400 uncertainty intervals of the monthly mean frequencies were caused by inter-annual variability  
401 (Fig. 2), and they are also influenced by the absolute number of NPF event days in separate  
402 months, which is substantially smaller in winter months than in the other months.

403

404

405

406

407

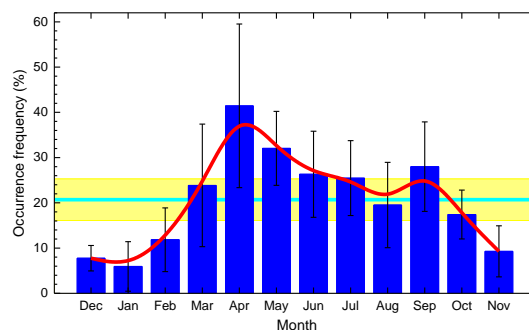
408

409

410

411

412



413

414

415

416

417

418

419

420

421

422

423

424

425

**Figure 3.** Mean distribution of the monthly mean relative occurrence frequency of NPF event days for the joint six-year-long data set in the city centre. The error bars show  $\pm 1$  SD, the horizontal line in cyan indicates the overall mean and the yellow band represents its  $\pm 1$  SD. The smooth curve in red serves to guide the eye.

It seems that the overall mean distribution does not change further extensively if another new year (for example Y8) is added into the data set. This is also the reason why Fig. 3 and a related plot which was presented earlier (Fig. 1 in Salma and Németh, 2019) are similar. This all implies that the shape of the overall distribution can already be considered to be representative. Moreover, it appears to be characteristic and remarkable. Furthermore, it closely agrees with a multi-year general shape even for some very diverse and detached environments such as boreal forest (Nieminen et al., 2014). It seems, therefore, to be sensible to study the factors that lead to this general structure. We chose to display the up-to-date overall distribution here to foster its comparison to that of environmental variables within the present article.

### 426 3.2 Distributions of environmental variables

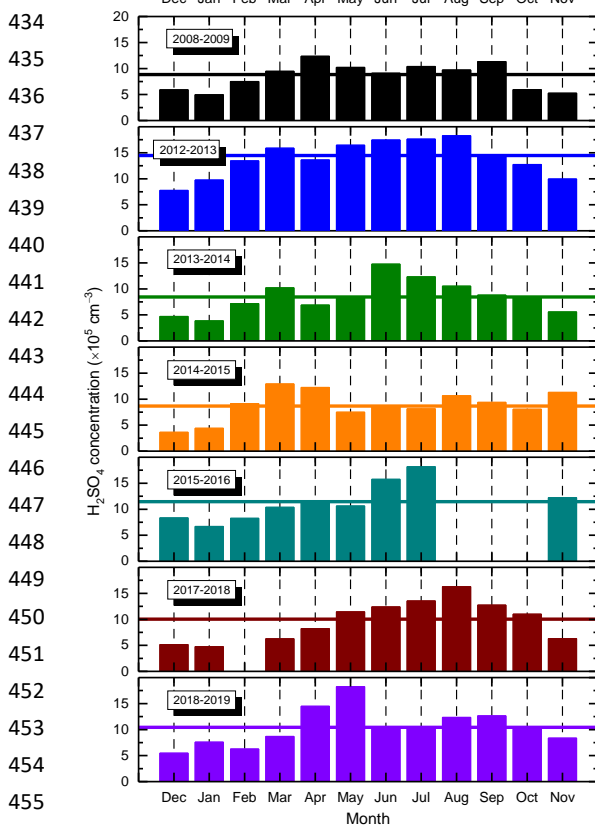
427 Distributions of the monthly mean values for environmental variables for the seven  
428 measurement years were derived. The pots for  $\text{H}_2\text{SO}_4$  concentration are shown in Fig. 4 as  
429 example. The distributions for some other selected variables, i.e. of  $\text{SO}_2$ ,  $\text{GRad}_{\text{max}}$ , CS,  $\text{O}_3$ ,



430 NO<sub>2</sub>, NH<sub>3</sub>, RH, WS and *T* are presented in Figs. S2–S10, respectively. The monthly averages  
431 which are missing in these figures were not available.

432

433



456 **Figure 4.** Distribution of monthly median gas-phase H<sub>2</sub>SO<sub>4</sub> concentration for the seven measurement years. The  
457 values for August–October 2016 and February 2018 are not available. The horizontal lines indicate annual  
458 medians. The measurements in 2012–2013 were performed in the near-city background, while in the other years,  
459 they were accomplished in the city centre.

460

461 By comparing Figs. 4 and 2, we can conclude that there are similar overall tendencies in their  
462 shape for several years. The concentration of H<sub>2</sub>SO<sub>4</sub> also tended to have a maximum in spring  
463 and another one in August or September. Its seasonal variation could jointly be affected mainly  
464 by [SO<sub>2</sub>], CS and GRad (Petäjä et al. 2009). Concentration of SO<sub>2</sub> showed a maximum in winter  
465 (Fig. S2), GRad<sub>max</sub> had a broad and obvious maximum in summer (Fig. S3), while CS tended  
466 to exhibit minimum values in summer (Fig. S4). It seems that in the first approximation, the  
467 *f*<sub>NPF</sub> distribution is linked to the temporal cycling of H<sub>2</sub>SO<sub>4</sub> concentration. It does not explain,

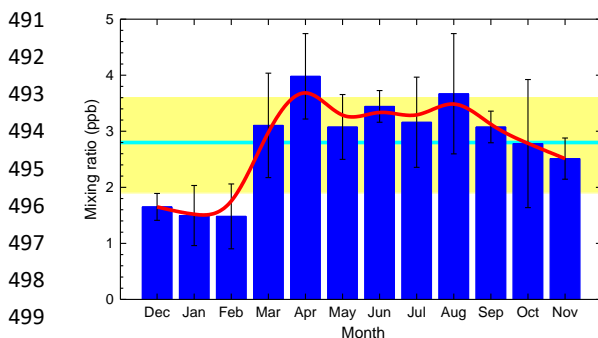


468 however, the temporal variability alone and other environmental variables have to play  
469 important roles in NPF occurrence.

470

471 For most of the other environmental properties, their connections with occurrence frequency  
472 were even weaker or featureless (than for  $[\text{H}_2\text{SO}_4]$  and  $f_{\text{NPF}}$  pair) with some similar tendencies  
473 reached in sporadic years. The only exception seemed to be  $\text{NH}_3$  concentration (Fig. S7). Its  
474 overall mean distribution was derived by averaging the data for the corresponding years, and  
475 it is shown in Fig. 5. The shape of the resulting distribution resembles the form and structure  
476 of the overall  $f_{\text{NPF}}$  distribution (cf. Fig. 3). It also contains an absolute maximum in April and  
477 an absolute minimum in January-February, and perhaps a local maximum in August. The  
478 situation is, however, complicated by the dissociation equilibrium in  $\text{NH}_4\text{NO}_3$  (solid or liquid),  
479  $\text{NH}_3$  (gas) and  $\text{HNO}_3$  (gas) thermodynamic system, which is rather sensitive to  $T$ ,  $\text{RH}$  and  
480 particle size or solution concentration and  $\text{pH}$  (Mozurkewich, 1993; Nenes et al., 2020).  
481 Ambient gas-phase  $[\text{NH}_3]$  are regulated and modified by this equilibrium as well. The  
482 similarities in the shapes and the coincidence in the extremes for the two variables may suggest  
483 that the availability of  $\text{NH}_3$  gas – as a base chemical compound in the atmosphere – can enhance  
484 the nucleation of  $\text{H}_2\text{SO}_4$  molecules in the ambient air thus, NPF event occurrence. This is in  
485 line with results from chamber experiments (Kirkby et al., 2011), while the involvement of  
486  $\text{NH}_3$  in NPF under relatively warm ambient conditions (close to the land surface in the  
487 atmosphere) has not been completely clarified yet (Kürten, 2019). It also raises a question  
488 whether other relevant atmospheric chemical bases such as amines have in general or in  
489 synergy with  $\text{NH}_3$  a similar role in the area.

490



491  
492  
493  
494  
495  
496  
497  
498  
499  
500 **Figure 5.** Mean distribution of the monthly mean  $\text{NH}_3$  mixing ratio for the joint six-year-long data set in the city  
501 centre. The error bars show  $\pm 1$  SD, the horizontal line in cyan indicates the overall mean and the yellow band  
502 represents its  $\pm 1$  SD. The smooth curve in red serves to guide the eye.



503 Pearson's coefficients of correlation between  $f_{\text{NPF}}$  and the other variables in the joined monthly  
504 mean data set were typically  $|R| < 0.50$ , except for RH,  $\text{GRad}_{\text{max}}$ , NO,  $\text{O}_3$  and  $\text{NH}_3$ , which were  
505  $-0.72$ ,  $0.70$ ,  $-0.61$ ,  $0.58$  and  $0.53$ , respectively. It is added that the variables influence the  
506 occurrence jointly, and, therefore, the pair wise correlation may not be fully satisfactory for  
507 revealing their relationships.

508

509 Another possible explanation of the characteristic structure could be related to the idea that  
510 NPF events often occur in elevated heights (as they are favoured at lower  $T$ s) and the nucleated  
511 particles are mixed down toward the land surface by general effects of turbulent mixing and  
512 air temperature which can have annual cycling. Dedicated measurements on this issue have  
513 been in progress to clarify this proposal (Carnerero et al., 2018).

### 514 3.3 Temperature anomaly

515 Possible impacts of  $T$  on NPF occurrence exerted indirectly through vegetation was further  
516 investigated by using anomalies. The anomaly emphasises the deviation of an environmental  
517 property (for a given time interval, here for a month or week) from its multi-year trend. The  
518 standardised anomaly is expressed in units of SD of the whole data set considered. The  
519 anomalies in maximum  $T$  and in NPF occurrence frequency were determined as described in  
520 Sec. 2.1, with SDs of  $3.1\text{ }^\circ\text{C}$  and  $13\%$ , respectively. Their time distributions (Fig. 6) resembled  
521 fluctuations as expected.

522

523 First, the possible impacts of standardised anomaly in maximum  $T$  above vegetated territories  
524 on the extreme values of monthly NPF occurrence frequency was examined. This can be  
525 achieved by comparing the column plots in Fig. 2 with the  $T$  anomaly lines in Fig. 6 for each  
526 year. (Their joint graph is shown in Fig. S11.) In many cases (e.g. in spring 2008, 2012, 2017  
527 and 2018), the absolute (spring) maximum of the occurrence frequency overlapped with or  
528 followed a substantial positive  $T$  anomaly. The exceptions were the years 2014–2015 (Y4) and  
529 2015–2016 (Y5). This suggests that NPF events are generally favoured or possibly are linked  
530 to larger  $T$ s in spring. The impact of  $T$  is, however, part of more comprehensive environmental  
531 interactions. No similar observation could be made with respect to the absolute minimum  $f_{\text{NPF}}$ .  
532 This implies that the lowest NPF occurrence in winter is most likely not restricted by  $T$ .

533

534 The effect of the potential heat stress exerted on plants in sultry summer intervals has become  
535 a relevant issue in the Carpathian Basin because of climate change. During these extremely warm





536 intervals, the plants could emit less VOCs since their stomata are more closed to reduce the  
537 rate of transpiration (Sect. 2.2.1). The coincidence between the positive  $T$  anomaly and summer  
538 minimum  $f_{\text{NPF}}$  could not be, however, established in the present data set.

539

540

541

542

543

544

545

546

547

548

549

550

551

552

553

554

555

556

557

558

559

560

561

562

563

564

565

566

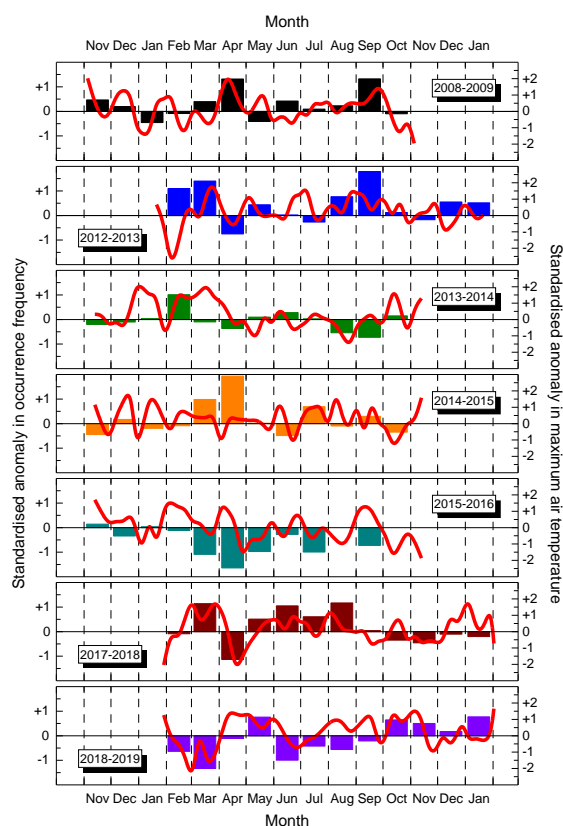
567

568

569

570

571



562 **Figure 6.** Time distribution of anomalies standardised to annual SD of the variable in maximum air temperature  
563 above vegetated territories (red lines) and in monthly mean NPF occurrence frequency (column charts) for the  
564 seven measurement years.

565

566 As the next step, the variability of the standardised anomaly in maximum  $T$  above vegetated  
567 territories and in monthly NPF occurrence frequency were investigated (Fig. 6) to assess the  
568 sensitivity of NPF to  $T$ . Some temporal tendencies between the two anomalies change in line  
569 although their variability seems loose or not coherent in some other intervals. This can partially  
570 be explained by multi-factorial impacts of environmental variables including vegetation-  
571 derived quantities. There could also be some delay in the relationship between  $T$  and  $f_{\text{NPF}}$ . It



572 emphasizes again the need for multi-variate statistical evaluation methods comprising cross-  
573 connections among the variables, which is going to be part of a next dedicated study.

574

575 In addition, the monthly or 8-d mean values evaluated so far do not necessary capture the  
576 potential relationships among the variables fully since they may take effect on shorter, e.g.  
577 daily time scale, which could be of not less importance from the point of NPF view. In order  
578 to extend our study to shorter time intervals, we continued investigating the daily mean data.

### 579 **3.4 Event-day-to-non-event-day ratios**

580 The monthly and annual mean ratios of the environmental variables on NPF event day and on  
581 non-event days in the city centre are summarised in Table 2. The relative occurrence  
582 frequencies of event days were also given for comparative purposes. The ratios can be  
583 influenced again by the number of event days. The uncertainty of the ratios for the modelled  
584 variable could be as high as 30 % or even larger if the monthly mean data are relatively small  
585 (e.g. for GPP, LAI and SCT in winter). The variables with annual ratios of approximately  
586  $r_{an}>1.1$  can be considered to favour or to be associated with NPF occurrence in general, the  
587 variables with approximately  $r_{an}<0.9$  can be regarded to disfavouring events, while the  
588 variables with  $r_{an}$  between these two limits possibly have low influence on NPF.

589

590 It is the  $H_2SO_4$  that shows the largest annual mean ratio. The atmospheric concentration of  
591  $H_2SO_4$  was larger by a factor of ca. 1.5 on event days than on non-event day. The ratio was  
592 even larger in winter months (a mean factor of 1.8) over which the other chemical and  
593 meteorological conditions for NPF are less favourable than in general. In winter, NPF events  
594 happen if  $H_2SO_4$  is available in relatively large excess concentrations which can ensure the  
595 required supersaturation. For all the other months, the mean ratios were also larger than unity.  
596 The smallest monthly mean ratio was obtained in July (and possibly in August and September).  
597 This all confirms the primary role of  $H_2SO_4$  in the phenomenon.

598

599 The second largest annual mean ratio was found for  $O_3$ . Its larger concentrations are often  
600 associated with general photochemical activity and secondary organic aerosol (SOA) formation  
601 (McFiggans et al., 2019). Its influence – represented by the ratio of the monthly mean event-  
602 day-to-non-event-day ratio to its annual mean ratio – in winter was the largest (1.64) of all  
603 relative ratios. This all implies that the photochemical reactivity, involving e.g. the  $H_2SO_4$



604 formation in the gas phase and the VOC oxidation, also plays an important role particularly in  
 605 those months when the absolute oxidative property is relatively low (Fig. S5 for O<sub>3</sub>).

606

607 **Table 2.** Overall mean relative occurrence frequency of NPF event days ( $f_{\text{NPF}}$  in percent) and overall mean event-  
 608 day-to-non-event-day ratios for daily median concentration of gas-phase H<sub>2</sub>SO<sub>4</sub> and O<sub>3</sub>, daily maximum GRad  
 609 (GRad<sub>max</sub>),  $N_{6-100}$ ,  $N$ , WS, gross primary production (GPP) of vegetation, stomatal conductance (SCT), SO<sub>2</sub>, leaf  
 610 area index (LAI), NO<sub>2</sub>,  $P$ , NO, NH<sub>3</sub>, PM<sub>10</sub> mass, CO, CS,  $N_{100-1000}$  and RH for each month and for all data in the  
 611 city centre. The ratios were organised in descending order of their annual mean values (the first data column).  
 612

Interval/ Variable	Annual	Dec	Jan	Feb	Mar	Apr	May	Jun	Jul	Aug	Sep	Oct	Nov
$f_{\text{NPF}}$	21	7.8	5.9	11.8	24	41	32	26	25	17.0	26	17.4	9.3
H <sub>2</sub> SO <sub>4</sub>	1.54	1.61	2.2	1.66	1.38	1.40	1.35	1.40	1.19	1.29	1.29	1.59	1.56
O <sub>3</sub>	1.42	2.6	2.6	1.79	1.20	0.99	1.09	1.18	0.97	1.07	0.99	1.26	1.28
GRad <sub>max</sub>	1.32	1.71	1.56	1.47	1.24	1.26	1.19	1.12	1.05	1.17	1.13	1.44	1.48
$N_{6-100}$	1.25	1.06	0.88	1.18	1.11	1.60	1.46	1.13	1.21	1.52	1.38	1.20	1.28
$N$	1.17	0.92	0.78	1.08	1.05	1.52	1.40	1.10	1.15	1.44	1.31	1.10	1.19
WS	1.16	1.68	1.66	1.23	1.18	0.92	0.97	1.14	1.15	0.77	0.97	1.21	1.00
GPP	1.14	1.47	0.99	1.06	1.20	1.20	1.12	0.98	1.06	1.06	0.97	0.90	1.72
SCT	1.10	1.22	1.11	0.98	1.17	1.08	0.97	0.95	1.16	1.01	1.04	0.90	1.61
SO <sub>2</sub>	1.08	0.88	0.82	1.01	1.05	1.20	1.18	1.18	1.09	1.22	1.11	1.05	1.20
LAI	1.05	0.98	1.02	1.01	1.16	1.05	1.01	0.97	1.04	0.98	0.99	0.82	1.54
NO <sub>2</sub>	1.02	0.93	0.86	1.00	0.86	1.15	1.18	0.95	0.89	1.13	1.09	1.05	1.09
$P$	1.00	1.00	1.00	1.00	1.00	1.00	1.00	1.00	1.00	1.00	1.00	1.00	1.00
NO	0.99	0.65	0.52	0.80	0.95	1.25	1.37	0.88	0.92	1.03	1.18	1.07	1.19
NH <sub>3</sub>	0.96	0.90	0.91	0.88	0.82	1.04	1.12	1.03	0.86	0.86	1.03	1.14	0.93
PM <sub>10</sub>	0.95	0.71	0.71	0.87	0.81	1.08	1.16	1.05	0.99	1.01	1.08	0.94	1.02
CO	0.94	0.78	0.69	0.88	0.89	1.06	1.03	1.01	0.90	0.95	1.08	0.90	1.10
CS	0.90	0.53	0.55	0.77	0.82	1.17	1.16	0.95	0.91	1.20	1.04	0.78	0.97
$N_{100-1000}$	0.89	0.50	0.53	0.78	0.82	1.16	1.14	0.97	0.90	1.18	1.03	0.77	0.97
RH	0.87	0.78	0.85	0.83	0.93	0.88	0.85	0.89	0.90	0.85	0.92	0.86	0.91

613

614 The GRad<sub>max</sub> exhibited the third largest annual mean ratio, and its monthly mean ratios were  
 615 also above unity. This property is related to the both variables discussed above and, therefore,  
 616 those arguments are valid here as well. It was shown that the presence of clouds decreases the  
 617 probability of NPF occurrence by attenuating solar radiation intensity below the cloud layer  
 618 (Baranizadeh et al., 2014; Dada et al., 2017), and that an ongoing event can even be interrupted  
 619 by a sudden appearance of clouds (Hirsikko et al., 2013; Salma et al., 2016a).

620

621 The large annual mean ratios for  $N$  and in particular for  $N_{6-100}$  are rather consequences of NPF  
 622 events than their causes. Ultrafine (UF) particles are generated by NPF and growth processes



623 in a large number. It is worth noting that the largest ratios of 1.5–1.6 happened in April, May  
624 and August, while the smallest ratio, which was below unity (0.88), was realised in January.  
625 This can partially be linked to the monthly variation of the particle formation and growth rates  
626 in Budapest as well (Salma and Németh, 2019). The interpretations of these ratios are in line  
627 with our earlier assessments or findings according to which 1) the concentrations of particles  
628 are increased by a factor of 2–3 on event days in central Budapest and 2) the NPF contribution  
629 as a single source of UF particles is ca. 13 % as a lower estimate and on longer run (Salma et  
630 al., 2017).

631

632 The effect of WS seems to be also noteworthy. On annual scale, higher WSs can be related to  
633 larger event occurrences. The distribution of its monthly mean, however, reveals a more  
634 complex relationship. In the months with large relative occurrence frequency (i.e. in April,  
635 May and September), the mean ratios were below unity (0.92 in April), in the winter months,  
636 they were extensively above unity (1.52), while they were very close to unity in the other  
637 months. This behaviour will be explained later in connection with CS and  $N_{100-1000}$ .

638

639 Precursor BVOC gases – approximated by GPP, LAI and SCT – and  $\text{SO}_2$  may generally favour  
640 NPF occurrence although their influence could not be quantified and seems to be low. The  
641 reason for this could partially be that the oxidation rates of precursors appear to be more  
642 important than their atmospheric concentrations (Salma and Németh, 2019), and that the effect  
643 of photochemical processes could be delayed in time. The concentrations of BVOCs are  
644 expected to be considerable in Budapest in spring. The typical mean contribution of biogenic  
645 sources to the total carbon in the  $\text{PM}_{2.5}$  size fraction was the second largest with a share of ca.  
646 40 % (Salma et al., 2020). Unfortunately, there is no experimental information available on  
647 absolute concentrations or amounts of VOC in the area. The effects of  $\text{NO}_2$ ,  $P$  and  $\text{NO}$  seemed  
648 to be even more constrained. Concentrations of  $\text{CO}$  and  $\text{PM}_{10}$  mass are often accounted as  
649 surrogates for urban air quality; and the polluted air seems to suppress NPF occurrence through  
650 high CS. Again, the monthly mean event-day-to-non-event-day ratios for  $\text{NO}$ ,  $\text{PM}_{10}$  mass and  
651  $\text{CO}$  were the smallest (typically 0.66, 0.76 and 0.78, respectively) in winter, when the  
652 preconditions of events are reached in a more difficult manner.

653

654 The mean ratios of CS and  $N_{100-1000}$  were close to each other and mostly below unity. Their  
655 lowest values of around 0.53 were reached in December and January. This implies that the NPF  
656 events preferably took place in winter on those days when the concentrations of pre-existing



657 particles were relatively small. The whole issue can be explained if considering that the basic  
658 preconditions of NPF events are realised by competing sources and sinks for condensing  
659 vapours. The source strength in winter is generally low due to lower solar radiation intensities  
660 and less biogenic precursor gases in the air. New particle formation events can occur at these  
661 low source intensities if the condensation and scavenging sinks – which are related to low  
662 particle number concentrations – are even smaller (Lehtinen et al., 2007). This can happen, for  
663 instance, due to a stronger wind (Fig. S9) which brings in low concentrations of regional and  
664 chemically aged particles ( $N_{100-1000}$ ) into city centres. The reasoning above is in line with and  
665 confirm our earlier findings related to diurnal and seasonal variations of UF particles (Salma  
666 et al., 2014, 2017).

667

668 The smallest annual mean event-day-to-non-event-day ratio was obtained for RH. All monthly  
669 mean ratios were also below unity and were similar to each other with an annual mean and SD  
670 of  $0.87 \pm 0.04$  (cf. Fig. S8). This unambiguously indicates that RH counteracts to NPF  
671 occurrence. It can serve as scavenger for OH radical (Petäjä et al., 2009). The dependency was  
672 already observed in earlier studies on continental NPF processes (Hamed et al., 2011).

673

674 It is noted for completeness that the mean event day minus non-event day  $T$  difference in the  
675 city centre for various months were 1.2 (Dec), 0.4 (Jan),  $-0.8$  (Feb), 0.4 (Mar), 1.5 (Apr), 1.9  
676 (May), 0.1 (Jun),  $-0.8$  (Jul), 0.1 (Aug),  $-0.5$  (Sep), 1.8 (Oct) and 1.4 °C (Nov). (The mean  
677 event-day-to-non-event-day ratios for  $T$  in a unit of K were all 1.00.) The monthly mean air  
678 temperature data do not indicate obvious relationships with  $f_{\text{NPF}}$  (cf. also Fig. S10). This is  
679 contrasting with its effect on NPF dynamic properties, for which the  $T$  causes summer maxima  
680 (Lee et al., 2019; Salma and Németh, 2019). The latter effect can be facilitated, for instance,  
681 through gas-phase auto-oxidation reactions involved in HOMs formation (Frege et al., 2018).  
682 The monthly and annual mean ratios of  $[\text{NH}_3]/\text{CS}$ ,  $\text{GPP}/\text{CS}$ ,  $\text{LAI}/\text{CS}$  and  $\text{SCT}/\text{CS}$  on NPF event  
683 days and on non-event days in the city centre were also derived considering that  $\text{NH}_3$  and  
684 BVOCs could in principle play a driving role in the events. The monthly ratios did not exhibit  
685 tendentious variation and did not resemble the distribution of occurrence frequency (Fig. 3).  
686 This and the concentration ratios for  $\text{NH}_3$  do not explicitly support the indications on its  
687 possible outstanding role (Sect. 3.2) and, therefore, further dedicated systematic studies are  
688 required in the area to arrive at conclusive overall interpretation of  $\text{NH}_3$ . The plans should  
689 preferably comprise other chemical species as well such as BVOCs or anthropogenic organics.



690 It is added that the effect of an environmental variable can depend on its absolute value as well.  
691 This can exhibit seasonal or other variability in time (Kerminen et al., 2018). The absolute  
692 values can also change from site to site and, furthermore, there can be different interactions or  
693 biases among some variables at different sites. Moreover, even dominant nucleation or growth  
694 mechanisms can vary at a fixed location depending on the availability of precursors or of  
695 different types of oxidation agents (e.g. OH, O<sub>3</sub> or NO<sub>3</sub>, Bianchi et al., 2016). These all factors  
696 can modify the effect of a variable. Strictly speaking, the interpretations above are, therefore,  
697 related to the region investigated. These aspects likely explain why the effects of some  
698 variables were interpreted inconclusively. For instance, both higher (Birmili and Wiedensohler  
699 2000; Zhao et al., 2015) and lower (Wu et al., 2007) SO<sub>2</sub> concentrations on event days relative  
700 to non-event days were reported at diverse locations.

### 701 3.5 Vegetation growth

702 The SoS and the GuD data are summarised in Table 3 for all vegetation. It is seen that the  
703 spring typically starts in the Budapest area around 28 March, and that the green-up of  
704 vegetation takes ordinary 40 days. These characteristics were, however, diverse when different  
705 vegetation types were considered. The SoS increased monotonically in the order of croplands,  
706 grasslands and forests. The spring started 2–3 days earlier for cultivated crops than for all  
707 vegetation, the start was almost identical for grass and all vegetation, while it was delayed by  
708 ca. 9 days for forest with respect to all vegetation. At the same time, the GuD for grasslands  
709 and croplands were identical (42–43 d), while the green-up was faster by 32 % for forests (27 d)  
710 than for all vegetation. This all can likely be explained by phyto-physiological properties of  
711 the different plants, seeding routine of cultivated crops and increasing intensity of solar  
712 radiation (and *T*) in the course of springtime.

713

714 **Table 3.** Start of spring (SoS) with its SD and the green-up duration (GuD) with its SD for all vegetation within  
715 a 100-km diameter circular area around Budapest for all measurement years. The years in brackets indicate the  
716 calendar year of the spring.

717

Property	Year/ Unit	Y1 (2009)	Y2 (2012)	Y3 (2014)	Y4 (2015)	Y5 (2016)	Y6 (2017)	Y7 (2018)	Y8 (2019)	Mean
SoS	date	02 Apr	03 Apr	18 Mar	30 Mar	26 Mar	25 Mar	02 Apr	23 Mar	28 Mar
SoS	day of year	92	94	78	89	86	84	92	82	87
SD	d	12	14	17	18	17	12	15	16	–
GuD	d	33	39	42	43	42	41	32	49	40
SD	d	18	15	20	18	19	16	17	19	–



718 The scatter plot of the SoS date for all vegetation and the start of NPF event occurrence spring  
719 peak is shown in Fig. 7. It is recalled that the measurements in 2012–2013 (Y2) were conducted  
720 in a forest clearing in the near-city background (Sect. 2.1), and that the growth characteristics  
721 are different for various vegetation types as just concluded above. For this reason, the data  
722 point for year Y2 was excluded from the further evaluations. We kept displaying it in Fig. 7,  
723 but it is shown in a different (black) colour from the other points to emphasize this. It is seen  
724 that the NPF spring occurrence reacted more sensitively than the visible vegetation spring or  
725 green-up in general. This outcome agrees with our long-term sensing perceptions. More  
726 importantly, a clear relationship between the NPF and SoS timing could be identified. The  
727 Pearson's coefficient of correlation of the data set was  $R=0.80$ . Their link was expressed by a  
728 linear fit utilizing weighted least-squares method. The goodness of the fit was quantified by  
729 the coefficient of determination, which was  $R^2=0.63$ . The statistical quantities above support  
730 that the association between vegetation dynamics and NPF occurrence is significant. We are  
731 aware that the two properties are likely biased by other variables such as e.g. GRad, and,  
732 therefore, the interpretation of their causal relationship or direct links are subject to further  
733 dedicated investigations.

734

735

736

737

738

739

740

741

742

743

744

745

746

747

748

749

750

751

752

753

754

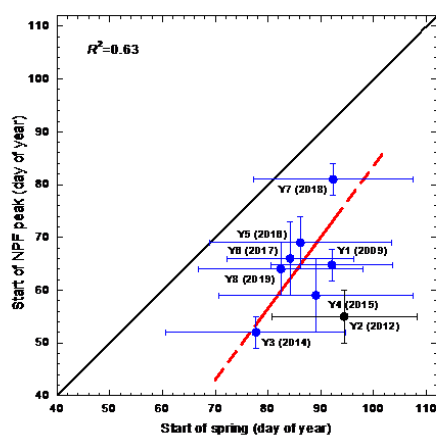


**Figure 7.** Scatter plot of the start of spring date considering all vegetation and the start of NPF occurrence spring season (peak). Labels for the measurement years Y1–Y8 and the calendar year of their spring (in brackets) are also shown. The error bars indicate  $\pm 1$  SD. The solid red line represents the linear fit, while its dashed parts were obtained by extrapolation. The data point for Y2 (2012) in black colour represents a forested environment, and, therefore, it was excluded from the fitting. The coefficient of determination ( $R^2$ ) for the fit is also given. The line of equality is displayed in black colour for orientating purpose only.



755 The relationships of GuD for all vegetation and the total number of NPF events in spring, the  
756 maximum monthly occurrence frequency in spring and the monthly mean occurrence  
757 frequency in spring are shown in Fig. S12a–c, respectively. The data points imply that the  
758 vegetation growth rate does not affected the NPF spring characteristics. This could suggest that  
759 a faster vegetation green-up, which is expectedly connected also to generally larger  
760 concentrations of BVOCs, does not appear to influence the NPF occurrence.

#### 761 **4 Conclusions**

762 Annual mean NPF occurrence frequencies in a continental Central European area were  
763 considerable (with an overall mean of 21 %), remained at a constant level (with a overall SD  
764 of 5 %) and did not exhibit tendentious change over 2008–2018. The shapes of the distributions  
765 of monthly mean occurrence frequency for the years varied substantially. The overall mean  
766 distribution, however, possessed a pattern. Its structure was likely caused by multifactorial  
767 influences of environmental properties. The most important components quantified in this  
768 ambient study included gas-phase H<sub>2</sub>SO<sub>4</sub>, O<sub>3</sub>, GRad, WS, CS and RH. The factors also  
769 involved precursor gases of vapours and their photochemical transformation processes.

770

771 A large fraction of chemical compounds contributing to NPF events in cities is expected to  
772 originate from anthropogenic precursors. Their emissions may peak any time of year depending  
773 on urban activities and human habits. Nevertheless, the  $f_{\text{NPF}}$  distributions seem to follow a  
774 general spring maximum and winter minimum behaviour. This could be associated with a very  
775 universal and widespread phenomenon. Emissions from vegetation or availability of (biogenic)  
776 atmospheric chemical bases can be involved. We investigated here the role of some vegetation-  
777 related factors in combination with environmental influencing properties in ambient NPF  
778 process. This approach represents a noteworthy novelty. We showed that there are several  
779 important links between the plant phenology in the area and event occurrence as far as both  
780 their timing properties and some absolute measures/magnitudes are concerned. Tight pair wise  
781 relationships between  $f_{\text{NPF}}$  on one hand and a large variety of environmental variables on the  
782 other hand could not be, however, proved. This suggests that the environmental players  
783 comprising vegetation exert their impact in a joint manner as a sensitive outcome of interacting  
784 components.

785





786 The relationships between vegetation and NPF can further be investigated at a molecular level  
787 utilising long-term advanced/sophisticated on-line mass spectrometry of organic chemical  
788 species of vegetation origin among precursors, nucleating vapours and in molecular clusters.  
789 Understanding these very complex and internally interacting multicomponent chemical  
790 mixtures also requires complementing field and laboratory studies with modelling.

791 *Data availability.* The observational data are available from the corresponding author upon reasonable request.

792 *Supplement.* The supplement related to this article is available online.

793 *Author contributions.* IS designed and organised the research study. WT, PA, ZB and IS performed and assisted  
794 in most aerosol and meteorological measurements. WT accomplished most of the data treatment and prepared  
795 most figures. AK derived and evaluated the products from MODIS, temperature anomaly data and created the  
796 maps in Fig. 1. ZB calculated the Biome-BGCMuSo results. IS, MK, VMK, AK and ZB interpreted the results.  
797 IS wrote the manuscript with comments from all coauthors.

798 *Competing interests.* The authors declare that they have no conflict of interest.

799 *Acknowledgements.* The authors thank Z. Németh and T. Weidinger both of the Eötvös University for their  
800 assistance. We are grateful to L. Horváth and K. Labacz of the Hungarian Meteorological Service for providing  
801 the  $\text{NH}_3$  concentrations.

802 *Financial support.* This research has been supported by the Hungarian Research, Development and Innovation  
803 Office (grant nos. K116788, FK128709 and K132254), by the European Regional Development Fund and the  
804 Hungarian Government (GINOP-2.3.2-15-2016-00028), by the Advanced research supporting the forestry and  
805 wood-processing sector's adaptation to global change and the 4th industrial revolution (grant no.  
806 CZ.02.1.01/0.0/0.0/16\_019/0000803 financed by OP RDE), by the Academy of Finland (Center of Excellence in  
807 Atmospheric Sciences, grant no. 4100104), and by the ERC Advanced Grant ATM-GTP (grant no. 742206).

## 808 References

- 809 Almeida, J., Schobesberger, S., Kurten, A., Ortega, I. K., Kupiainen-Maatta, O., Praplan, A. P., Adamov, A.,  
810 Amorim, A., Bianchi, F., Breitenlechner, M., David, A., Dommen, J., Donahue, N. M., Downard, A., Dunne,  
811 E., Duplissy, J., Ehrhart, S., Flagan, R. C., Franchin, A., Guida, R., Hakala, J., Hansel, A., Heinritzi, M.,  
812 Henschel, H., Jokinen, T., Junninen, H., Kajos, M., Kangasluoma, J., Keskinen, H., Kupc, A., Kurten, T.,  
813 Kvashin, A. N., Laaksonen, A., Lehtipalo, K., Leiminger, M., Leppa, J., Loukonen, V., Makhmutov, V.,  
814 Mathot, S., McGrath, M. J., Nieminen, T., Olenius, T., Onnela, A., Petäjä, T., Riccobono, F., Riipinen, I.,  
815 Rissanen, M., Rondo, L., Ruuskanen, T., Santos, F. D., Sarnela, N., Schallhart, S., Schnitzhofer, R.,  
816 Seinfeld, J. H., Simon, M., Sipilä, M., Stozhkov, Y., Stratmann, F., Tome, A., Tröstl, J., Tsagkogeorgas, G.,  
817 Vaattovaara, P., Viisanen, Y., Virtanen, A., Vrtala, A., Wagner, P. E., Weingartner, E., Wex, H.,  
818 Williamson, C., Wimmer, D., Ye, P. L., Yli-Juuti, T., Carslaw, K. S., Kulmala, M., Curtius, J.,  
819 Baltensperger, U., Worsnop, D. R., Vehkamäki, H., and Kirkby, J.: Molecular understanding of sulphuric  
820 acid–amine particle nucleation in the atmosphere, *Nature*, 502, 359–363, 2013.
- 821 Baranzadeh, E., Arola, A., Hamed, A., Nieminen, T., Mikkonen, S., Virtanen, A., Kulmala, M., Lehtinen, K.,  
822 and Laaksonen, A.: The effect of cloudiness on new-particle formation: investigation of radiation levels  
823 *Boreal Environ. Res.*, 19, 343–54, 2014.
- 824 Barcza, Z., Bondeau, A., Churkina, G., Ciais, Ph., Czóbel, Sz., Gelybó, Gy., Grosz, B., Haszpra, L., Hidy, D.,  
825 Horváth, L., Machon, A., Pásztor, L., Somogyi, Z., and Van Oost, K.: Modeling of biosphere-atmosphere  
826 exchange of greenhouse gases - Model based biospheric greenhouse gas balance of Hungary, in:  
827 *Atmospheric Greenhouse Gases: The Hungarian Perspective* (ed.: Haszpra, L.), Springer, Dordrecht, 295–  
828 330, doi:10.1007/978-90-481-9950-1, 2010.
- 829 Bianchi, F., Tröstl, J., Junninen, H., Frege, C., Henne, S., Hoyle, C. R., Molteni, U., Herrmann, E., Adamov, A.,  
830 Bukowiecki, N., Chen, X., Duplissy, J., Gysel, M., Hutterli, M., Kangasluoma, J., Kontkanen, J., Kürten, A.,  
831 Manninen, H. E., Münch, S., Peräkylä, O., Petäjä, T., Rondo, L., Williamson, C., Weingartner, E., Curtius, J.,  
832 Worsnop, D. R., Kulmala, M., Dommen, J., and Baltensperger, U.: New particle formation in the free  
833 troposphere: A question of chemistry and timing, *Science*, 352, 1109–1112, 2016.



- 834 Birmili, W. and Wiedensohler, A.: New particle formation in the continental boundary layer: meteorological and  
835 gas phase parameter influence, *Geophys. Res. Lett.*, 27, 3325–3328, 2000.
- 836 Bonan, G.: *Ecological Climatology: concepts and applications*, Cambridge University Press, Cambridge,  
837 doi:10.1017/CBO9781107339200, 2015.
- 838 Bousiotis, D., Dall'Osto, M., Beddows, D. C. S., Pope, F. D., and Harrison, R. M.: Analysis of new particle  
839 formation (NPF) events at nearby rural, urban background and urban roadside sites, *Atmos. Chem. Phys.*, 19,  
840 5679–5694, 2019.
- 841 Boy, M. and Kulmala, M.: Nucleation events in the continental boundary layer: Influence of physical and  
842 meteorological parameters, *Atmos. Chem. Phys.*, 2, 1–16, 2002.
- 843 Braakhuis, H. M., Park, M. V., Gosens, I., De Jong, W. H., and Cassee, F. R.: Physicochemical characteristics  
844 of nanomaterials that affect pulmonary inflammation, *Part. Fibre Toxicol.*, 11:18, doi:10.1186/1743-8977-  
845 11-18, 2014.
- 846 Brines, M., Dall'Osto, M., Beddows, D. C. S., Harrison, R. M., Gómez-Moreno, F., Núñez, L., Artíñano, B.,  
847 Costabile, F., Gobbi, G. P., Salimi, F., Morawska, L., Sioutas, C., and Querol, X.: Traffic and nucleation  
848 events as main sources of ultrafine particles in high-insolation developed world cities, *Atmos. Chem. Phys.*,  
849 15, 5929–5945, 2015.
- 850 Carnerero, C., Pérez, N., Reche, C., Ealo, M., Titos, G., Lee, H.-K., Eun, H.-R., Park, Y.-H., Dada, L.,  
851 Paasonen, P., Kerminen, V.-M., Mantilla, E., Escudero, M., Gómez-Moreno, F. J., Alonso-Blanco, E., Coz,  
852 E., Saiz-Lopez, A., Temime-Roussel, B., Marchand, N., Beddows, D. C. S., Harrison, R. M., Petäjä, T.,  
853 Kulmala, M., Ahn, K.-H., Alastuey, A., and Querol, X.: Vertical and horizontal distribution of regional new  
854 particle formation events in Madrid, *Atmos. Chem. Phys.*, 18, 16601–16618, 2018.
- 855 Carslaw, K. S., Lee, L. A., Reddington, C. L., Pringle, K. J., Rap, A., Forster, P. M., Mann, G. W., Spracklen,  
856 D. V., Woodhouse, M. T., Regayre, L. A., and Pierce, J. R.: Large contribution of natural aerosols to  
857 uncertainty in indirect forcing, *Nature*, 503, 67–71, 2013.
- 858 Cornes, R., Van Der Schrier, G., Van Den Besselaar, E. J. M., and Jones, P. D.: An ensemble version of the E  
859 OBS temperature and precipitation datasets, *J. Geophys. Res. Atmos.*, 123, 9391–9409, 2018.
- 860 Clement, C. F., Pirjola, L., Dal Maso, M., Mäkelä, J., and Kulmala, M.: Analysis of particle formation bursts  
861 observed in Finland, *J. Aerosol Sci.*, 32, 217–36, 2001.
- 862 Dada, L., Paasonen, P., Nieminen, T., Buenrostro Mazon, S., Kontkanen, J., Peräkylä, O., Lehtipalo, K.,  
863 Hussein, T., Petäjä, T., Kerminen, V.-M., Bäck, J., and Kulmala, M.: Long-term analysis of clear-sky new  
864 particle formation events and nonevents in Hyytiälä, *Atmos. Chem. Phys.*, 17, 6227–6241, 2017.
- 865 Dada, L., Ylivinkka, I., Baalbaki, R., Li, Ch., Guo, Y., Yan, Ch., Yao, L., Sarnela, N., Jokinen, T., Daellenbach,  
866 K. D., Yin, R., Deng, Ch., Chu, B., Nieminen, T., Kontkanen, J., Stolzenburg, D., Sipilä, M., Hussein, T.,  
867 Paasonen, P., Bianchi, F., Salma, I., Weidinger, T., Pikridas, M., Sciare, J., Jiang, J., Liu, Y., Petäjä, T.,  
868 Kerminen, V.-M., and Kulmala, M.: Sources and sinks driving sulphuric acid concentrations in contrasting  
869 environments: implications on proxy calculations, *Atmos. Chem. Phys. Discuss.*,  
870 <https://doi.org/10.5194/acp-2020-155>, in review, 2020.
- 871 Dal Maso, M., Kulmala, M., Lehtinen, K. E. J., Mäkelä, J. M., Aalto, P. P., and O'Dowd, C.: Condensation and  
872 coagulation sinks and formation of nucleation mode particles in coastal and boreal forest boundary layers, *J.*  
873 *Geophys. Res.*, 107(19D), 8097, 10.1029/2001jd001053, 2002.
- 874 Dal Maso, M., Kulmala, M., Riipinen, I., Wagner, R., Hussein, T., Aalto, P. P., and Lehtinen, K. E. J.:  
875 Formation and growth of fresh atmospheric aerosols: eight years of aerosol size distribution data from  
876 SMEAR II, Hyytiälä, Finland, *Boreal Environ. Res.*, 10, 323–336, 2005.
- 877 Dall'Osto, M., Querol, X., Alastuey, A., O'Dowd, C., Harrison, R. M., Wenger, J., and Gómez-Moreno, F. J.: On  
878 the spatial distribution and evolution of ultrafine particles in Barcelona, *Atmos. Chem. Phys.*, 13, 741–759,  
879 2013.
- 880 Dall'Osto, M., Beddows, D. C. S., Asmi, A., Poulain, L., Hao, L., Freney, E., Allan, J. D., Canagaratna, M.,  
881 Crippa, M., Bianchi, F., De Leeuw, G., Eriksson, A., Swietlicki, E., Hansson, H. C., Henzing, J. S., Granier,  
882 C., Zemanekova, K., Laj, P., Onasch, T., Prevot, A., Putaud, J. P., Sellegri, K., Vidal, M., Virtanen, A., Simo,  
883 R., Worsnop, D., O'Dowd, C., Kulmala, M., and Harrison, R. M.: Novel insights on new particle formation  
884 derived from a pan-European observing system, *Sci. Reports*, 8, 1482, 01.12.2018, 2018.
- 885 Dobor, L., Barcza, Z., Hlásny, T., Havasi, A., Horváth, F., Ittész, P., and Bartholy, J.: Bridging the gap between  
886 climate models and impact studies: the FORESEE Database, *Geosci. Data J.*, 2, 1–11, 2014.
- 887 Donahue, N. M., Ortega, I. K., Chuang, W., Riipinen, I., Riccobono, F., Schobesberger, S., Dommen, J.,  
888 Baltensperger, U., Kulmala, M., and Worsnop, D. R.: How do organic vapors contribute to new-particle  
889 formation?, *Faraday Discuss.*, 165, 91–104, 2013.
- 890 Dunne, E., Gordon, H., Kürten, A., Almeida, J., Duplissy, J., Williamson, Ch., Ortega, I., Pringle, K., Adamov,  
891 A., Baltensperger, U., Barmet, P., Benduhn, F., Bianchi, F., Breitenlechner, M., Clarke, A., Curtius, J.,  
892 Dommen, J., Donahue, N., Ehrhart, S., and Carslaw, K.: Global atmospheric particle formation from CERN  
893 CLOUD measurements, *Science*, 354, 10.1126/science.aaf2649, 2016.



- 894 Ehn, M., Thornton, J. A., Kleist, E., Sipilä, M., Junninen, H., Pullinen, I., Springer, M., Rubach, F., Tillmann,  
895 R., Lee, B., Lopez-Hilfiker, F., Andres, S., Acir, I. H., Rissanen, M., Jokinen, T., Schobesberger, S.,  
896 Kangasluoma, J., Kontkanen, J., Nieminen, T., Kurten, T., Nielsen, L. B., Jorgensen, S., Kjaergaard, H. G.,  
897 Canagaratna, M., Dal Maso, M., Berndt, T., Petäjä, T., Wahner, A., Kerminen, V. M., Kulmala, M.,  
898 Worsnop, D. R., Wildt, J., and Mentel, T. F.: A large source of low-volatility secondary organic aerosol,  
899 *Nature*, 506, 476–479, 2014.
- 900 EMEP (Co-operative Programme for Monitoring and Evaluation of the Long-range Transmission of Air  
901 Pollutants in Europe) Manual, Chemical Co-ordination Centre Report 1/2002, Norwegian Institute for Air  
902 Research, Kjeller, 2002.
- 903 Erupe, M. E., Viggiano, A. A., and Lee, S.-H.: The effect of trimethylamine on atmospheric nucleation  
904 involving H<sub>2</sub>SO<sub>4</sub>, *Atmos. Chem. Phys.*, 11, 4767–4775, 2011.
- 905 Farquhar, G. D., von Caemmerer, S., and Berry, J. A.: A bio-chemical model of photosynthetic CO<sub>2</sub> assimilation  
906 in leaves of C3 species, *Planta*, 149, 78–90, 1980.
- 907 Frege, C., Ortega, I. K., Rissanen, M. P., Praplan, A. P., Steiner, G., Heinritzi, M., Ahonen, L., Amorim, A.,  
908 Bernhammer, A.-K., Bianchi, F., Brilke, S., Breitenlechner, M., Dada, L., Dias, A., Duplissy, J., Ehrhart, S.,  
909 El-Haddad, I., Fischer, L., Fuchs, C., Garmash, O., Gonin, M., Hansel, A., Hoyle, C. R., Jokinen, T.,  
910 Junninen, H., Kirkby, J., Kürten, A., Lehtipalo, K., Leiminger, M., Mauldin, R. L., Molteni, U., Nichman,  
911 L., Petäjä, T., Sarnela, N., Schobesberger, S., Simon, M., Sipilä, M., Stolzenburg, D., Tomé, A., Vogel, A.  
912 L., Wagner, A. C., Wagner, R., Xiao, M., Yan, C., Ye, P., Curtius, J., Donahue, N. M., Flagan, R. C.,  
913 Kulmala, M., Worsnop, D. R., Winkler, P. M., Dommen, J., and Baltensperger, U.: Influence of temperature  
914 on the molecular composition of ions and charged clusters during pure biogenic nucleation, *Atmos. Chem.*  
915 *Phys.*, 18, 65–79, 2018.
- 916 Gordon, H., Sengupta, K., Rap, A., Duplissy, J., Frege, C., Williamson, C., Heinritzi, M., Simon, M., Yan, C.,  
917 Almeida, J., Tröstl, J., Nieminen, T., Ortega, I. K., Wagner, R., Dunne, E. M., Adamov, A., Amorim, A.,  
918 Bernhammer, A. K., Bianchi, F., Breitenlechner, M., Brilke, S., Chen, X., Craven, J. S., Dias, A., Ehrhart, S.,  
919 Fischer, L., Flagan, R. C., Franchin, A., Fuchs, C., Guida, R., Hakala, J., Hoyle, C. R., Jokinen, T., Junninen,  
920 H., Kangasluoma, J., Kim, J., Kirkby, J., Krapf, M., Kürten, A., Laaksonen, A., Lehtipalo, K., Makhmutov,  
921 V., Mathot, S., Molteni, U., Monks, S. A., Onnela, A., Peräkylä, O., Piel, F., Petäjä, T., Praplan, A. P.,  
922 Pringle, K. J., Richards, N. A. D., Rissanen, M. P., Rondo, L., Sarnela, N., Schobesberger, S., Scott, C. E.,  
923 Seinfeld, J. H., Sharma, S., Sipilä, M., Steiner, G., Stozhkov, Y., Stratmann, F., Tomé, A., Virtanen, A.,  
924 Vogel, A. L., Wagner, A. C., Wagner, P. E., Weingartner, E., Wimmer, D., Winkler, P. M., Ye, P., Zhang,  
925 X., Hansel, A., Dommen, J., Donahue, N. M., Worsnop, D. R., Baltensperger, U., Kulmala, M., Curtius, J.,  
926 and Carslaw, K. S.: Reduced anthropogenic aerosol radiative forcing caused by biogenic new particle  
927 formation, *Proc. Natl. Acad. Sci. U.S.A.*, 113, 12053–12058, <https://doi.org/10.1073/pnas.1602360113>,  
928 2016.
- 929 Hamed, A., Korhonen, H., Sihto, S.-L., Joutsensaari, J., Järvinen, H., Petäjä, T., Arnold, F., Nieminen, T.,  
930 Kulmala, M., Smith, J. N., Lehtinen, K. E. J., and Laaksonen, A.: The role of relative humidity in continental  
931 new particle formation, *J. Geophys. Res.*, 116, D03202, doi:10.1029/2010JD014186, 2011.
- 932 He, X.-Ch., Tham, Y. J., Dada, L., Wang, M., Finkenzeller, H., Stolzenburg, D., Simon, M., Shen, J., Rörup, B.,  
933 Iyer, S., Rissanen, M., Schobesberger, S., Baalbaki, R., Wang, D. S., Koenig, T. K., Jokinen, T., Sarnela, N.,  
934 Beck, L., Almeida, J., Kürten, A., Amanatidis, S., Amorim, A., Ataei, F., Baccarini, A., Bertozzi, B., Brilke,  
935 S., Caudillo, L., Chen, D., Chiu, R., Chu, B., Dias, A., Ding, A., Dommen, J., Duplissy, J., El Haddad, I.,  
936 Flagan, R. C., Carracedo, L. G., Granzin, M., Hansel, A., Heinritzi, M., Hofbauer, V., Junninen, H.,  
937 Kangasluoma, J., Kempainen, D., Kim, Ch., Kong, W., Krechmer, J. E., Kvashnin, A., Laitinen, T.,  
938 Lamkaddam, H., Lee, Ch. P., Lehtipalo, K., Leiminger, M., Li, Z., Makhmutov, V., Manninen, H. E., Marie,  
939 G., Marten, R., Mauldin, R. L., Mentler, B., Möhler, O., Müller, T., Nie, W., Onnela, A., Petäjä, T., Pfeifer,  
940 J., Philippov, M., Ranjithkumar, A., Salma, I., Scholz, W., Schuchmann, S., Schulze, B., Steiner, G.,  
941 Stozhkov, Y., Tauber, Ch., Tomé, A., Väisänen, O., Vazquez-Pufleau, M., Wagner, A. C., Wang, Y., Weber,  
942 S. K., Winkler, P. M., Wu, Y., Xiao, M., Yan, Ch., Ye, Q., Ylisirniö, A., Zauner-Wieczorek, M., Zha, Q.,  
943 Zhou, P., Curtius, J., Baltensperger, U., Kulmala, M., Kerminen, V.-M., Kurtén, T., Donahue, N. M.,  
944 Volkamer, R., Kirkby, J., Worsnop, D. R., and Sipilä, M.: Global significance of iodine acid new-particle  
945 formation in the atmosphere, submitted in 2020.
- 946 Heinritzi, M., Dada, L., Simon, M., Stolzenburg, D., Wagner, A. C., Fischer, L., Ahonen, L. R., Amanatidis, S.,  
947 Baalbaki, R., Baccarini, A., Bauer, P. S., Baumgartner, B., Bianchi, F., Brilke, S., Chen, D., Chiu, R., Dias,  
948 A., Dommen, J., Duplissy, J., Finkenzeller, H., Frege, C., Fuchs, C., Garmash, O., Gordon, H., Granzin, M.,  
949 Haddad, I. E., He, X., Helm, J., Hofbauer, V., Hoyle, C. R., Kangasluoma, J., Keber, T., Kim, C., Kürten, A.,  
950 Lamkaddam, H., Lampilahti, J., Laurila, T. M., Lee, C. P., Lehtipalo, K., Leiminger, M., Mai, H.,  
951 Makhmutov, V., Manninen, H. E., Marten, R., Mathot, S., Mauldin, R. L., Mentler, B., Molteni, U., Müller,  
952 T., Nie, W., Nieminen, T., Onnela, A., Partoll, E., Passananti, M., Petäjä, T., Pfeifer, J., Pospisilova, V.,  
953 Quéléver, L., Rissanen, M. P., Rose, C., Schobesberger, S., Scholz, W., Scholze, K., Sipilä, M., Steiner, G.,  
954 Stozhkov, Y., Tauber, C., Tham, Y. J., Vazquez-Pufleau, M., Virtanen, A., Vogel, A. L., Volkamer, R.,



- 955 Wagner, R., Wang, M., Weitz, L., Wimmer, D., Xiao, M., Yan, C., Ye, P., Zha, Q., Zhou, X., Amorim, A.,  
956 Baltensperger, U., Hansel, A., Kulmala, M., Tomé, A., Winkler, P. M., Worsnop, D. R., Donahue, N. M.,  
957 Kirkby, J., and Curtius, J.: Molecular understanding of the suppression of new-particle formation by  
958 isoprene, *Atmos. Chem. Phys. Discuss.*, <https://doi.org/10.5194/acp-2020-51>, in review, 2020.
- 959 Hidy, D., Barcza, Z., Marjanović, H., Ostrogović Sever, M. Z., Dobor, L., Gelybó, G., Fodor, N., Pintér, K.,  
960 Churkina, G., Running, S., Thornton, P., Bellocchi, G., Haszpra, L., Horváth, F., Suyker, A., and Nagy, Z.:  
961 Terrestrial ecosystem process model Biome-BGCMuSo v4.0: summary of improvements and new modeling  
962 possibilities, *Geosci. Model Dev.*, 9, 4405–4437, 2016.
- 963 Hirsikko, A., Vakkari, V., Tiitta, P., Manninen, H. E., Gagné, S., Laakso, H., Kulmala, M., Mirme, A., Mirme,  
964 S., Mabaso, D., Beukes, J. P., and Laakso, L.: Characterisation of sub-micron particle number concentrations  
965 and formation events in the western Bushveld Igneous Complex, South Africa, *Atmos. Chem. Phys.*, 12,  
966 3951–3967, 2012.
- 967 Hirsikko, A., Vakkari, V., Tiitta, P., Hatakka, J., Kerminen, V.-M., Sundström, A.-M., Beukes, J. P., Manninen,  
968 H. E., Kulmala, M., and Laakso, L.: Multiple daytime nucleation events in semi-clean savannah and  
969 industrial environments in South Africa: analysis based on observations, *Atmos. Chem. Phys.*, 13, 5523–  
970 5532, 2013.
- 971 Horváth, L., Fagerli, H., and Sutton, M. A.: Long-term record (1981–2005) of ammonia and ammonium  
972 concentrations at K-pusztá, Hungary and the effect of sulphur dioxide emission change on measured and  
973 modelled concentrations, In: Sutton M. A., Reis S., and Baker S. M. (eds): *Atmospheric ammonia*. Springer,  
974 Dordrecht, 2009.
- 975 Jokinen, T., Berndt, T., Makkonen, R., Kerminen, V.-M., Junninen, H., Paasonen, P., Stratmann, F., Herrmann,  
976 H., Guenther, A. B., Worsnop, D. R., Kulmala, M., Ehn, M. and Sipilä, M.: Production of extremely low  
977 volatile organic compounds from biogenic emissions: Measured yields and atmospheric implications, *Proc.*  
978 *Natl. Acad. Sci. U.S.A.*, 112, 7123–7128, 2015.
- 979 Justice, C. O., Vermote, E., Townshend, J. R. G., Defries, R., Roy, D. P., Hall, D. K., Salomonson, V. V.,  
980 Privette, J. L., Riggs, G., Strahler, A., Lucht, W., Myneni, R., Knjazihhin, Y., Running, S., Nemani, R.,  
981 Wan, Z., Huete, A., vanLeeuwen, W., Wolfe, R., Giglio, L., Muller, J.-P., Lewis, P., and Barnsley, M.: The  
982 Moderate Resolution Imaging Spectroradiometer (MODIS): land remote sensing for global change research,  
983 *Trans. Geosci. Remote Sens.*, 36, 1228–1249, 1998.
- 984 Jun, Y.-S., Jeong, C.-H., Sabaliauskas, K., Leaith, W. R., and Evans, G. J.: A year-long comparison of particle  
985 formation events at paired urban and rural locations, *Atmos. Pollut. Res.*, 5, 447–54, 2014.
- 986 Kerminen, V.-M., Paramonov, M., Anttila, T., Riipinen, I., Fountoukis, C., Korhonen, H., Asmi, E., Laakso, L.,  
987 Lihavainen, H., Swietlicki, E., Svenningsson, B., Asmi, A., Pandis, S. N., Kulmala, M., and Petäjä, T.:  
988 Cloud condensation nuclei production associated with atmospheric nucleation: a synthesis based on existing  
989 literature and new results, *Atmos. Chem. Phys.*, 12, 12037–12059, 2012.
- 990 Kerminen, V.-M., Chen, X., Vakkari, V., Petäjä, T., Kulmala, M., and Bianchi, F.: Atmospheric new particle  
991 formation and growth: review of field observations, *Environ. Res. Lett.*, 13 (2018) 103003, 2018.
- 992 Kern, A., Marjanović, H., and Barcza, Z.: Evaluation of the quality of NDVI3g dataset against Collection 6  
993 MODIS NDVI in Central-Europe between 2000 and 2013, *Remote Sens.*, 8, 955, doi:10.3390/rs8110955,  
994 2016.
- 995 Kern, A., Marjanović, H., and Barcza, Z.: Spring vegetation green-up dynamics in Central Europe based on 20-  
996 year long MODIS NDVI data, *Agric. For. Met.*, 287, 107969, doi:10.1016/j.agrformet.2020.107969, 2020.
- 997 Kiendler-Scharr, A., Wildt, J., Dal Maso, M., Hohaus, T., Kleist, E., Mentel, T. F., Tillmann, R., Uerlings, R.,  
998 Schurr, U., and Wahner, A.: New particle formation in forests inhibited by isoprene emissions, *Nature*, 461,  
999 381–384, 2009.
- 1000 Kirkby, J., Curtius, J., Almeida, J., Dunne, E., Duplissy, J., Ehrhart, S., Franchin, A., Gagné, S., Ickes, L.,  
1001 Kürten, A., Kupc, A., Metzger, A., Riccobono, F., Rondo, L., Schobesberger, S., Tsagkogeorgas, G.,  
1002 Wimmer, D., Amorim, A., Bianchi, F., Breitenlechner, M., David, A., Dommen, J., Downard, A., Ehn, M.,  
1003 Flagan, R. C., Haider, S., Hansel, A., Hauser, D., Jud, W., Junninen, H., Kreissl, F., Kvashin, A., Laaksonen,  
1004 A., Lehtipalo, K., Lima, J., Lovejoy, E. R., Makhutov, V., Mathot, S., Mikkilä, J., Minginette, P., Mogo, S.,  
1005 Nieminen, T., Onnela, A., Pereira, A., Petäjä, T., Schnitzhofer, R., Seinfeld, J. H., Sipilä, M., Stozhkov, Y.,  
1006 Stratmann, F., Tome, A., Vanhanen, J., Viisanen, Y., Vrtala, A., Wagner, P. E., Walther, H., Weingartner, E.,  
1007 Wex, H., Winkler, P. M., Carslaw, K. S., Worsnop, D. R., Baltensperger, U., and Kulmala, M.: The role of  
1008 sulfuric acid, ammonia and galactic cosmic rays in atmospheric aerosol nucleation, *Nature*, 476, 429–433,  
1009 2011.
- 1010 Kirkby, J., Duplissy, J., Sengupta, K., Frege, C., Gordon, H., Williamson, C., Heinritzi, M., Simon, M., Yan, C.,  
1011 Almeida, J., Tröstl, J., Nieminen, T., Ortega, I. K., Wagner, R., Adamov, A., Amorim, A., Bernhammer, A.-  
1012 K., Bianchi, F., Breitenlechner, M., Brilke, S., Chen, X., Craven, J., Dias, A., Ehrhart, S., Flagan, R. C.,  
1013 Franchin, A., Fuchs, C., Guida, R., Hakala, J., Hoyle, C. R., Jokinen, T., Junninen, H., Kangasluoma, J.,  
1014 Kim, J., Krapf, M., Kürten, A., Laaksonen, A., Lehtipalo, K., Makhmutov, V., Mathot, S., Molteni, U.,  
1015 Onnela, A., Peräkylä, O., Piel, F., Petäjä, T., Praplan, A. P., Pringle, K., Rap, A., Richards, N. A. D.,



- 1016 Riipinen, I., Rissanen, M. P., Rondo, L., Sarnela, N., Schobesberger, S., Scott, C. E., Seinfeld, J. H., Sipilä,  
1017 M., Steiner, G., Stozhkov, Y., Stratmann, F., Tomé, A., Virtanen, A., Vogel, A. L., Wagner, A., Wagner, P.  
1018 E., Weingartner, E., Wimmer, D., Winkler, P. M., Ye, P., Zhang, X., Hansel, A., Dommen, J., Donahue, N.  
1019 M., Worsnop, D. R., Baltensperger, U., Kulmala, M., Carslaw, K. S., and Curtius, J.: Ion-induced nucleation  
1020 of pure biogenic particles, *Nature*, 533, 521–526, 2016.
- 1021 Kulmala, M., Petäjä, T., Nieminen, T., Sipilä, M., Manninen, H. E., Lehtipalo, K., Dal Maso, M., Aalto, P. P.,  
1022 Junninen, H., Paasonen, P., Riipinen, I., Lehtinen, K. E. J., Laaksonen, A., and Kerminen, V.-M.:  
1023 Measurement of the nucleation of atmospheric aerosol particles, *Nat. Protoc.*, 7, 1651–1667, 2012.
- 1024 Kulmala, M., Kontkanen, J., Junninen, H., Lehtipalo, K., Manninen, H. E., Nieminen, T., Petäjä, T., Sipilä, M.,  
1025 Schobesberger, S., Rantala, P., Franchin, A., Jokinen, T., Järvinen, E., Äijälä, M., Kangasluoma, J., Hakala,  
1026 J., Aalto, P. P., Paasonen, P., Mikkilä, J., Vanhanen, J., Aalto, J., Hakola, H., Makkonen, U., Ruuskanen, T.,  
1027 Mauldin, R. L. III, Duplissy, J., Vehkamäki, H., Bäck, J., Kortelainen, A., Riipinen, I., Kurtén, T., Johnston,  
1028 M. V., Smith, J. N., Ehn, M., Mentel, T. F., Lehtinen, K. E. J., Laaksonen, A., Kerminen, V.-M., and  
1029 Worsnop, D. R.: Direct observations of atmospheric aerosol nucleation, *Science*, 339, 943–946, 2013.
- 1030 Kulmala, M., Petäjä, T., Ehn, M., Thornton, J., Sipilä, M., Worsnop, D. R., and Kerminen, V.-M.: Chemistry of  
1031 atmospheric nucleation: On the recent advances on precursor characterization and atmospheric cluster  
1032 composition in connection with atmospheric new particle formation, *Annu. Rev. Phys. Chem.*, 65, 21–37,  
1033 2014.
- 1034 Kulmala, M., Kerminen, V. M., Petäjä, T., Ding, A. J., and Wang, L.: Atmospheric gas-to-particle conversion:  
1035 why NPF events are observed in megacities, *Faraday Discuss.*, doi:10.1039/C6FD00257A, 2017.
- 1036 Kürten, A.: New particle formation from sulfuric acid and ammonia: nucleation and growth model based on  
1037 thermodynamics derived from CLOUD measurements for a wide range of conditions, *Atmos. Chem. Phys.*,  
1038 19, 5033–5050, 2019.
- 1039 Lee, S.-H., Gordon, H., Yu, H., Lehtipalo, K., Haley, R., Li, Y., and Zhang, R.: New particle formation in the  
1040 atmosphere: from molecular clusters to global climate, *J. Geophys. Res. Atmos.*, 124, 7098–7146, 2019.
- 1041 Lehtinen, K. E. J., Dal Maso, M., Kulmala, M., and Kerminen, V.-M.: Estimating nucleation rates from apparent  
1042 particle formation rates and vice versa: Revised formulation of the Kerminen-Kulmala equation, *J. Aerosol  
1043 Sci.*, 38, 988–994, 2007.
- 1044 Lehtipalo, K., Rondo, L., Kontkanen, J., Schobesberger, S., Jokinen, T., Sarnela, N., Kürten, A., Ehrhart, S.,  
1045 Franchin, A., Nieminen, T., Riccobono, F., Sipilä, M., Yli-Juuti, T., Duplissy, J., Adamov, A., Ahlm, L.,  
1046 Almeida, J., Amorim, A., Bianchi, F., Breitenlechner, M., Dommen, J., Downard, A. J., Dunne, E. M.,  
1047 Flagan, R. C., Guida, R., Hakala, J., Hansel, A., Jud, W., Kangasluoma, J., Kerminen, V.-M., Keskinen, H.,  
1048 Kim, J., Kirkby, J., Kupc, A., Kupiainen-Määttä, O., Laaksonen, A., Lawler, M. J., Leiminger, M., Mathot,  
1049 S., Olenius, T., Ortega, I. K., Onnela, A., Petäjä, T., Praplan, A., Rissanen, M. P., Ruuskanen, T., Santos, F.  
1050 D., Schallhart, S., Schnitzhofer, R., Simon, M., Smith, J. N., Tröstl, J., Tsagkogeorgas, G., Tomé, A.,  
1051 Vaattovaara, P., Vehkamäki, H., Virtala, A. E., Wagner, P. E., Williamson, C., Wimmer, D., Winkler, P. M.,  
1052 Virtanen, A., Donahue, N. M., Carslaw, K. S., Baltensperger, U., Riipinen, I., Curtius, J., Worsnop, D. R.  
1053 and Kulmala, M.: The effect of acid-base clustering and ions on the growth of atmospheric nano-particles,  
1054 *Nat. Commun.*, 7, 11594, <https://doi.org/10.1038/ncomms11594>, 2016.
- 1055 Lehtipalo, K., Yan, C., Dada, L., Bianchi, F., Xiao, M., Wagner, R., Stolzenburg, D., Ahonen, L. R., Amorim,  
1056 A., Baccarini, A., Bauer, P. S., Baumgartner, B., Bergen, A., Bernhammer, A.-K., Breitenlechner, M.,  
1057 Brilke, S., Buchholz, A., Mazon, S. B., Chen, X., Dias, A., Dommen, J., Draper, D. C., Duplissy,  
1058 J., Ehn, M., Finkenzeller, H., Fischer, L., Frege, C., Fuchs, C., Garmash, O., Gordon, H., Hakala, J., He, X.,  
1059 Heikkinen, L., Heinritzi, M., Helm, J. C., Hofbauer, V., Hoyle, C. R., Jokinen, T., Kangasluoma, J.,  
1060 Kerminen, V.-M., Kim, C., Kirkby, J., Kontkanen, J., Kürten, A., Lawler, M. J., Mai, H., Mathot, S.,  
1061 Mauldin, R. L., Molteni, U., Nichman, L., Nie, W., Nieminen, T., Ojdanic, A., Onnela, A., Passananti, M.,  
1062 Petäjä, T., Piel, F., Pospisilova, V., Quéléver, L. L. J., Rissanen, M. P., Rose, C., Sarnela, N., Schallhart, S.,  
1063 Schuchmann, S., Sengupta, K., Simon, M., Sipilä, M., Tauber, C., Tomé, A., Tröstl, J., Väisänen, O., Vogel,  
1064 A. L., Volkamer, R., Wagner, A. C., Wang, M., Weitz, L., Wimmer, D., Ye, P., Ylisirmö, A., Zha, Q.,  
1065 Carslaw, K. S., Curtius, J., Donahue, N. M., Flagan, R. C., Hansel, A., Riipinen, I., Virtanen, A., Winkler, P.  
1066 M., Baltensperger, U., Kulmala, M., and Worsnop, D. R.: Multicomponent new particle formation from  
1067 sulfuric acid, ammonia, and biogenic vapors, *Sci. Adv.*, 4, eaau5363, <https://doi.org/10.1126/sciadv.aau5363>,  
1068 2018.
- 1069 LP DAAC (Land Processes Distributed Active Archive Center), MOD09A1, Collection 6, NASA EOSDIS  
1070 Land Processes DAAC, USGS Earth Resources Observation and Science (EROS) Center, Sioux Falls, South  
1071 Dakota, 2019. URL: <https://lpdaac.usgs.gov>, accessed on 14 January 2020.
- 1072 Makkonen, R., Asmi, A., Korhonen, H., Kokkola, H., Järvenoja, S., Räisänen, P., Lehtinen, K. E. J., Laaksonen,  
1073 A., Kerminen, V.-M., Järvinen, H., Lohmann, U., Bennartz, R., Feichter, J., and Kulmala, M.: Sensitivity of  
1074 aerosol concentrations and cloud properties to nucleation and secondary organic distribution in ECHAM5-  
1075 HAM global circulation model, *Atmos. Chem. Phys.*, 9, 1747–1766, 2009.



- 1076 Makkonen, R., Asmi, A., Kerminen, V.-M., Boy, M., Arneth, A., Hari, P., and Kulmala, M.: Air pollution  
1077 control and decreasing new particle formation lead to strong climate warming, *Atmos. Chem. Phys.*, 12,  
1078 1515–1524, 2012.
- 1079 Manninen, H. E., Nieminen, T., Asmi, E., Gagné, S., Häkkinen, S., Lehtipalo, K., Aalto, P., Vana, M., Mirme,  
1080 A., Mirme, S., Hörrak, U., Plass-Dülmer, C., Stange, G., Kiss, G., Hoffer, A., Törö, N., Moerman, M.,  
1081 Henzig, B., de Leeuw, G., Brinkenberg, M., Kouvarakis, G. N., Bougiatioti, A., Mihalopoulos, N.,  
1082 O’Dowd, C., Ceburnis, D., Arneth, A., Svenningsson, B., Swietlicki, E., Tarozzi, L., Decesari, S., Facchini,  
1083 M. C., Birmili, W., Sonntag, A., Wiedensohler, A., Boulon, J., Sellegri, K., Laj, P., Gysel, M., Bukowiecki,  
1084 N., Weingartner, E., Wehrle, G., Laaksonen, A., Hamed, A., Joutsensaari, J., Petäjä, T., Kerminen, V.-M. and  
1085 Kulmala, M.: EUCAARI ion spectrometer measurements at 12 European sites – analysis of new particle  
1086 formation events, *Atmos. Chem. Phys.*, 10, 7907–7927, 2010.
- 1087 McFiggans, G., Mentel, T. F., Wildt, J., Pullinen, I., Kang, S., Kleist, E., Schmitt, S., Springer, M., Tillmann, R.,  
1088 Wu, C., Zhao, D., Hallquist, M., Faxon, C., Le Breton, M., Hallquist, A. M., Simpson, D., Bergstroem, R.,  
1089 Jenkin, M. E., Ehn, M., Thornton, J. A., Alfarra, M. R., Bannan, T. J., Percival, C. J., Priestley, M., Topping,  
1090 D., and Kiendler-Scharr, A.: Secondary organic aerosol reduced by mixture of atmospheric vapours, *Nature*,  
1091 565, 587–593, 2019.
- 1092 Meija, J. F. and Morawska, L.: An investigation of nucleation events in a coastal urban environment in the  
1093 Southern Hemisphere, *Atmos. Chem. Phys.*, 9, 7877–7888, 2009.
- 1094 Merikanto, J., Spracklen, D. V., Mann, G. W., Pickering, S. J., and Carslaw, K. S.: Impact of nucleation on  
1095 global CCN, *Atmos. Chem. Phys.*, 9, 8601–8616, 2009.
- 1096 Metzger, A., Verheggen, B., Dommen, J., Duplissy, J., Prévôt, A. S. H., Weingartner, E., Riipinen, I., Kulmala,  
1097 M., Spracklen, D. V., Carslaw, K. S., and Baltensperger, U.: Evidence for the role of organics in aerosol  
1098 particle formation under atmospheric conditions, *Proc. Natl. Acad. Sci. U. S. A.*, 107, 6646–6651, 2010.
- 1099 Mikkonen, S., Lehtinen, K. E. J., Hamed, A., Joutsensaari, J., Facchini, M. C., and Laaksonen, A.: Using  
1100 discriminant analysis as a nucleation event classification method, *Atmos. Chem. Phys.*, 6, 5549–5557, 2006.
- 1101 Mikkonen, S., Németh, Z., Varga, V., Weidinger, T., Leinonen, V., Yli-Juuti, T., and Salma, I.: Decennial time  
1102 trends and diurnal patterns of particle number concentrations in a Central European city between 2008 and  
1103 2018, *Atmos. Chem. Phys. Discuss.*, <https://doi.org/10.5194/acp-2020-305>, in review, 2020.
- 1104 Mozurkewich, M.: The dissociation constant of ammonium nitrate and its dependence on temperature, relative  
1105 humidity and particle size, *Atmos. Environ.*, 27A, 261–270, 1993.
- 1106 Németh, Z. and Salma, I.: Spatial extension of nucleating air masses in the Carpathian Basin, *Atmos. Chem.*  
1107 *Phys.*, 14, 8841–8848, 2014.
- 1108 Németh, Z., Rosati, B., Zíková, N., Salma, I., Bozó, L., Dameto de España, C., Schwarz, J., Ždímal, V., and  
1109 Wonaschütz, A.: Comparison of atmospheric new particle formation and growth events in three Central  
1110 European cities, *Atmos. Environ.*, 178, 191–197, 2018.
- 1111 Nenes, A., Pandis, S. N., Weber, R. J., and Russell, A.: Aerosol pH and liquid water content determine when  
1112 particulate matter is sensitive to ammonia and nitrate availability, *Atmos. Chem. Phys.*, 20, 3249–3258,  
1113 2020.
- 1114 Nieminen, T., Asmi, A., Dal Maso, M., P. Aalto, P., Keronen, P., Petäjä, T., Kulmala, M., and Kerminen, V.-M.:  
1115 Trends in atmospheric new-particle formation: 16 years of observations in a boreal-forest environment,  
1116 *Boreal Env. Res.*, 19 (suppl. B), 191–214, 2014.
- 1117 Nieminen, T., Kerminen, V.-M., Petäjä, T., Aalto, P. P., Arshinov, M., Asmi, E., Baltensperger, U., Beddows,  
1118 D. C. S., Beukes, J. P., Collins, D., Ding, A., Harrison, R. M., Henzing, B., Hooda, R., Hu, M., Hörrak, U.,  
1119 Kivekäs, N., Komsaare, K., Krejčí, R., Kristensson, A., Laakso, L., Laaksonen, A., Leitch, W. R.,  
1120 Lihavainen, H., Mihalopoulos, N., Németh, Z., Nie, W., O’Dowd, C., Salma, I., Sellegri, K., Svenningsson,  
1121 B., Swietlicki, E., Tunved, P., Ulevicvius, V., Vakkari, V., Vana, M., Wiedensohler, A., Wu, Z., Virtanen, A.,  
1122 and Kulmala, M.: Global analysis of continental boundary layer new particle formation based on long-term  
1123 measurements, *Atmos. Chem. Phys.*, 18, 14737–14756, 2018.
- 1124 O’Dowd, C. D., Jimenez, J. L., Bahreini, R., Flagan, R. C., Seinfeld, J. H., Hämeri, K., Pirjola, L., Kulmala, M.,  
1125 Jennings, S. G., and Hoffmann, Th.: Marine aerosol formation from biogenic iodine emissions, *Nature* 417,  
1126 632–636, 2002.
- 1127 Ohlwein, S., Kappeler, R., Joss, M. K., Künzli, N., and Hoffmann, B.: Health effects of ultrafine particles: a  
1128 systematic literature review update of epidemiological evidence, *Int. J. Public Health*, 685, 547–559, 2019.
- 1129 Petäjä, T., Mauldin, III, R. L., Kosciuch, E., McGrath, J., Nieminen, T., Paasonen, P., Boy, M., Adamov, A.,  
1130 Kotiaho, T., and Kulmala, M.: Sulfuric acid and OH concentrations in a boreal forest site, *Atmos. Chem.*  
1131 *Phys.*, 9, 7435–7448, 2009.
- 1132 Qian, S., Sakurai, H., and McMurry, P. H.: Characteristics of regional nucleation events in urban East St. Louis,  
1133 *Atmos. Environ.* 41 4119–4127, 2007.
- 1134 Riccobono, F., Schobesberger, S., Scott, C., Dommen, J., Ortega, I., Rondo, L., Almeida, J., Amorim, A.,  
1135 Bianchi, F., Breitenlechner, M., David, A., Downard, A., Dunne, E., Duplissy, J., Ehrhart, S., Flagan, R.,  
1136 Franchin, A., Hansel, A., Junninen, H., Kajos, M., Keskinen, H., Kupc, A., Kurten, A., Kvashin, A.,



- 1137 Laaksonen, A., Lehtipalo, K., Makhmutov, V., Mathot, S., Nieminen, T., Onnela, A., Petäjä, T., Praplan, A.,  
1138 Santos, F., Schallhart, S., Seinfeld, J., Sipilä, M., Spracklen, D., Stozhkov, Y., Stratmann, F., Tome, A.,  
1139 Tsagkogeorgas, G., Vaattovaara, P., Viisanen, Y., Vrtala, A., Wagner, P., Weingartner, E., Wex, H.,  
1140 Wimmer, D., Carslaw, K., Curtius, J., Donahue, N., Kirkby, J., Kulmala, M., Worsnop, D., and  
1141 Baltensperger, U.: Oxidation products of biogenic emissions contribute to nucleation of atmospheric  
1142 particles, *Science*, 344, 717–721, 2014.
- 1143 Riipinen, I., Pierce, J. R., Yli-Juuti, T., Nieminen, T., Häkkinen, S., Ehn, M., Junninen, H., Lehtipalo, K., Petäjä,  
1144 T., Slowik, J., Chang, R., Shantz, N. C., Abbatt, J., Leaitch, W. R., Kerminen, V.-M., Worsnop, D. R.,  
1145 Pandis, S. N., Donahue, N. M., and Kulmala, M.: Organic condensation: a vital link connecting aerosol  
1146 formation to cloud condensation nuclei (CCN) concentrations, *Atmos. Chem. Phys.*, 11, 3865–3878, 2011.
- 1147 Salma, I. and Németh, Z.: Dynamic and timing properties of new aerosol particle formation and consecutive  
1148 growth events, *Atmos. Chem. Phys.*, 19, 5835–5852, 2019.
- 1149 Salma, I., Borsós, T., Weidinger, T., Aalto, P., Hussein, T., Dal Maso, M., and Kulmala, M.: Production, growth  
1150 and properties of ultrafine atmospheric aerosol particles in an urban environment, *Atmos. Chem. Phys.*, 11,  
1151 1339–1353, 2011.
- 1152 Salma, I., Borsós, T., Németh, Z., Weidinger, T., Aalto, T., and Kulmala, M.: Comparative study of ultrafine  
1153 atmospheric aerosol within a city, *Atmos. Environ.*, 92, 154–161, 2014.
- 1154 Salma, I., Fűri, P., Németh, Z., Farkas, Á., Balásházy, I., Hofmann, W., and Farkas, Á.: Lung burden and  
1155 deposition distribution of inhaled atmospheric urban ultrafine particles as the first step in their health risk  
1156 assessment, *Atmos. Environ.*, 104, 39–49, 2015.
- 1157 Salma, I., Németh, Z., Weidinger, T., Kovács, B., and Kristóf, G.: Measurement, growth types and shrinkage of  
1158 newly formed aerosol particles at an urban research platform, *Atmos. Chem. Phys.*, 16, 7837–7851, 2016a.
- 1159 Salma, I., Németh, Z., Kerminen, V. M., Aalto, P., Nieminen, T., Weidinger, T., Molnár, Á., Imre, K., and  
1160 Kulmala, M.: Regional effect on urban atmospheric nucleation, *Atmos. Chem. Phys.*, 16, 8715–8728, 2016b.
- 1161 Salma, I., Varga, V., and Németh, Z.: Quantification of an atmospheric nucleation and growth process as a  
1162 single source of aerosol particles in a city, *Atmos. Chem. Phys.*, 17, 15007–15017, 2017.
- 1163 Salma, I., Vasanits-Zsigrai, A., Machon, A., Varga, T., Major, I., Gergely, V., and Molnár, M.: Fossil fuel  
1164 combustion, biomass burning and biogenic sources of fine carbonaceous aerosol in the Carpathian Basin,  
1165 *Atmos. Chem. Phys.*, 20, 4295–4312, 2020.
- 1166 Schobesberger, S., Junninen, H., Bianchi, F., Lonn, G., Ehn, M., Lehtipalo, K., Dommen, J., Ehrhart, S., Ortega,  
1167 I. K., Franchin, A., Nieminen, T., Riccobono, F., Hutterli, M., Duplissy, J., Almeida, J., Amorim, A.,  
1168 Breitenlechner, M., Downard, A. J., Dunne, E. M., Flagan, R. C., Kajos, M., Keskinen, H., Kirkby, J., Kupc,  
1169 A., Kurten, A., Kurten, T., Laaksonen, A., Mathot, S., Onnela, A., Praplan, A. P., Rondo, L., Santos, F. D.,  
1170 Schallhart, S., Schnitzhofer, R., Sipilä, M., Tome, A., Tsagkogeorgas, G., Vehkamäki, H., Wimmer, D.,  
1171 Baltensperger, U., Carslaw, K. S., Curtius, J., Hansel, A., Petäjä, T., Kulmala, M., Donahue, N. M., and  
1172 Worsnop, D. R.: Molecular understanding of atmospheric particle formation from sulfuric acid and large  
1173 oxidized organic molecules, *Proc. Natl. Acad. Sci. U.S.A.*, 110, 17223–17228, 2013.
- 1174 Shen, M., Piao, S., Cong, N., Zhang, G., and Jassens, I. A.: Precipitation impacts on vegetation spring  
1175 phenology on the Tibetan Plateau, *Glob. Chang. Biol.*, 21, 3647–3656, 2015.
- 1176 Seyednasrollah, B., Swenson, J. J., Domec, J. C., and Clark, J. S.: Leaf phenology paradox: Why warming  
1177 matters most where it is already warm, *Remote Sens. Environ.*, 209, 446–455, 2018.
- 1178 Sihto, S.-L., Kulmala, M., Kerminen, V.-M., Dal Maso, M., Petäjä, T., Riipinen, I., Korhonen, H., Arnold, F.,  
1179 Janson, R., Boy, M., Laaksonen, A., and Lehtinen, K. E. J.: Atmospheric sulphuric acid and aerosol  
1180 formation: implications from atmospheric measurements for nucleation and early growth mechanisms,  
1181 *Atmos. Chem. Phys.*, 6, 4079–4091, 2006.
- 1182 Sihto, S.-L., Mikkilä, J., Vanhanen, J., Ehn, M., Liao, L., Lehtipalo, K., Aalto, P. P., Duplissy, J., Petäjä, T.,  
1183 Kerminen, V.-M., Boy, M., and Kulmala, M.: Seasonal variation of CCN concentrations and aerosol  
1184 activation properties in boreal forest, *Atmos. Chem. Phys.*, 11, 13269–13285, 2011.
- 1185 Simon, M., Dada, L., Heinritzi, M., Scholz, W., Stolzenburg, D., Fischer, L., Wagner, A. C., Kürten, A., Rörup,  
1186 B., He, X.-C., Almeida, J., Baalbaki, R., Baccarini, A., Bauer, P. S., Beck, L., Bergen, A., Bianchi, F.,  
1187 Bräkling, S., Brilke, S., Caudillo, L., Chen, D., Chu, B., Dias, A., Draper, D. C., Duplissy, J., El Haddad, I.,  
1188 Finkenzeller, H., Frege, C., Gonzalez-Carracedo, L., Gordon, H., Granzin, M., Hakala, J., Hofbauer, V.,  
1189 Hoyle, C. R., Kim, C., Kong, W., Lamkaddam, H., Lee, C. P., Lehtipalo, K., Leiminger, M., Mai, H.,  
1190 Manninen, H. E., Marie, G., Marten, R., Mentler, B., Molteni, U., Nichman, L., Nie, W., Ojandic, A.,  
1191 Onnela, A., Partoll, E., Petäjä, T., Pfeifer, J., Philippov, M., Quéléver, L. L. J., Ranjithkumar, A., Rissanen,  
1192 M., Schallhart, S., Schobesberger, S., Schuchmann, S., Shen, J., Sipilä, M., Steiner, G., Stozhkov, Y.,  
1193 Tauber, C., Tham, Y. J., Tomé, A. R., Vazquez-Pufleau, M., Vogel, A., Wagner, R., Wang, M., Wang, D. S.,  
1194 Wang, Y., Weber, S. K., Wu, Y., Xiao, M., Yan, C., Ye, P., Ye, Q., Zauner-Wieczorek, M., Zhou, X.,  
1195 Baltensperger, U., Dommen, J., Flagan, R. C., Hansel, A., Kulmala, M., Volkamer, R., Winkler, P. M.,  
1196 Worsnop, D. R., Donahue, N. M., Kirkby, J., and Curtius, J.: Molecular understanding of new-particle



- 1197 formation from alpha-pinene between  $-50\text{ }^{\circ}\text{C}$  and  $25\text{ }^{\circ}\text{C}$ , *Atmos. Chem. Phys. Discuss.*,  
1198 <https://doi.org/10.5194/acp-2019-1058>, in review, 2020.
- 1199 Sipilä, M., Berndt, T., Petäjä, T., Brus, D., Vanhanen, J., Stratmann, F., Patokoski, J., Mauldin, R. L. 3rd,  
1200 Hyvärinen, A. P., Lihavainen, H., and Kulmala, M.: The role of sulfuric acid in atmospheric nucleation,  
1201 *Science*, 327, 1243–1246, 2010.
- 1202 Sipilä, M., Sarnela, N., Jokinen, T., Henschel, H., Junninen, H., Kontkanen, J., Richters, S., Kangasluoma, J.,  
1203 Franchin, A., Peräkylä, O., Rissanen, M. P., Ehn, M., Vehkamäki, H., Kurten, T., Berndt, T., Petäjä, T.,  
1204 Worsnop, D., Ceburnis, D., Kerminen, V.-M., Kulmala, M., and O'Dowd, C.: Molecular-scale evidence of  
1205 aerosol particle formation via sequential addition of  $\text{HIO}_3$ , *Nature*, 537, 532–534, 2016.
- 1206 Spracklen, D. V., Carslaw, K. S., Merikanto, J., Mann, G. W., Reddington, C. L., Pickering, S., Ogren, J. A.,  
1207 Andrews, E., Baltensperger, U., Weingartner, E., Boy, M., Kulmala, M., Laakso, L., Lihavainen, H.,  
1208 Kivekäs, N., Komppula, M., Mihalopoulos, N., Kouvarakis, G., Jennings, S. G., O'Dowd, C., Birmili, W.,  
1209 Wiedensohler, A., Weller, R., Gras, J., Laj, P., Sellegri, K., Bonn, B., Krejčí, R., Laaksonen, A., Hamed, A.,  
1210 Minikin, A., Harrison, R. M., Talbot, R., and Sun, J.: The contribution of boundary layer nucleation events  
1211 to total particle concentrations on regional and global scales, *Atmos. Chem. Phys.*, 6, 5631–5648, 2006.
- 1212 Sulla-Menashe, D. and Friedl, M. A.: User guide to collection 6 MODIS land cover (MCD12Q1 and  
1213 MCD12C1) product, Available online: [https://lpdaac.usgs.gov/sites/default/files/public/  
1214 product\\_documentation/mcd12\\_user\\_guide\\_v6.pdf](https://lpdaac.usgs.gov/sites/default/files/public/product_documentation/mcd12_user_guide_v6.pdf), 2018.
- 1215 Sun, J., Birmili, W., Hermann, M., Tuch, T., Weinhold, K., Spindler, G., Schladitz, A., Bastian, S., Löschau, G.,  
1216 Cyrys, J., Gu, J., Flentje, H., Briel, B., Asbach, C., Kaminski, H., Ries, L., Sohmer, R., Gerwig, H., Wirtz,  
1217 K., Meinhardt, F., Schwerin, A., Bath, O., Ma, N., and Wiedensohler, A.: Variability of Black Carbon mass  
1218 concentrations, sub-micrometer particle number concentrations and size distributions: Results of the German  
1219 Ultrafine Aerosol Network ranging from city street to high Alpine locations, *Atmos. Environ.*, 202, 256–268,  
1220 2019.
- 1221 Thornton, P. E. and Rosenbloom, N. A.: Ecosystem model spin-up: Estimating steady state conditions in a  
1222 coupled terrestrial carbon and nitrogen cycle model, *Ecol. Model.*, 189, 25–48, 2005.
- 1223 Tröstl, J., Chuang, W. K., Gordon, H., Heinritzi, M., Yan, C., Molteni, U., Ahlm, L., Frege, C., Bianchi, F.,  
1224 Wagner, R., Simon, M., Lehtipalo, K., Williamson, C., Craven, J. S., Duplissy, J., Adamov, A., Almeida, J.,  
1225 Bernhammer, A. K., Breitenlechner, M., Brilke, S., Dias, A., Ehrhart, S., Flagan, R. C., Franchin, A., Fuchs,  
1226 C., Guida, R., Gysel, M., Hansel, A., Hoyle, C. R., Jokinen, T., Junninen, H., Kangasluoma, J., Keskinen,  
1227 H., Kim, J., Krapf, M., Kürten, A., Laaksonen, A., Lawler, M., Leiminger, M., Mathot, S., Möhler, O.,  
1228 Nieminen, T., Onnela, A., Petäjä, T., Piel, F. M., Miettinen, P., Rissanen, M. P., Rondo, L., Sarnela, N.,  
1229 Schobesberger, S., Sengupta, K., Sipilä, M., Smith, J. N., Steiner, G., Tomè, A., Virtanen, A., Wagner, A.  
1230 C., Weingartner, E., Wimmer, D., Winkler, P. M., Ye, P. L., Carslaw, K. S., Curtius, J., Dommen, J., Kirkby,  
1231 J., Kulmala, M., Riipinen, I., Worsnop, D. R., Donahue, N. M., and Baltensperger, U.: The role of low-  
1232 volatility organic compounds in initial particle growth in the atmosphere, *Nature*, 533, 527,  
1233 10.1038/nature18271, 2016.
- 1234 Tunved, P., Hansson, H.-C., Kerminen, V.-M., Ström, J., Dal Maso, M., Lihavainen, H., Viisanen, Y., Aalto, P.  
1235 P., Komppula, M., and Kulmala, M.: High natural aerosol loading over boreal forest, *Science*, 312, 261–263,  
1236 2006.
- 1237 Vakkari, V., Laakso, H., Kulmala, M., Laaksonen, A., Mabaso, D., Molefe, M., Kgabi, N., and Laakso, L.: New  
1238 particle formation events in semi-clean South African savannah, *Atmos. Chem. Phys.*, 11, 3333–3346, 2011.
- 1239 Vermote, E.: MOD09A1 MODIS/Terra Surface Reflectance 8-Day L3 Global 500 m SIN Grid V006, NASA  
1240 EOSDIS Land Processes DAAC, 2015, accessed on 23 May 2018, doi: 10.5067/MODIS/MOD09A1.006.
- 1241 Wu, Z., Hu, M., Liu, S., Wehner, B., Bauer, S., Massling, A., Wiedensohler, A., Petäjä, T., Dal Maso, M. and  
1242 Kulmala, M.: New particle formation in Beijing, China: statistical analysis of a 1 year data set, *J. Geophys.  
1243 Res.*, 112, D09209, 2007.
- 1244 Xiao, S., Wang, M. Y., Yao, L., Kulmala, M., Zhou, B., Yang, X., Chen, J. M., Wang, D. F., Fu, Q. Y.,  
1245 Worsnop, D. R., and Wang, L.: Strong atmospheric new particle formation in winter in urban Shanghai,  
1246 China, *Atmos. Chem. Phys.*, 15, 1769–1781, 2015.
- 1247 Yao, L., Garmash, O., Bianchi, F., Zheng, J., Yan, C., Kontkanen, J., Junninen, H., Mazon, S. B., Ehn, M.,  
1248 Paasonen, P., Sipilä, M., Wang, M., Wang, X., Xiao, S., Chen, H., Lu, Y., Zhang, B., Wang, D., Fu, Q.,  
1249 Geng, F., Li, L., Wang, H., Qiao, L., Yang, X., Chen, J., Kerminen, V.-M., Petäjä, T., Worsnop, D. R.,  
1250 Kulmala, M., and Wang, L.: Atmospheric new particle formation from sulfuric acid and amines in a Chinese  
1251 megacity, *Science*, 361, 278–281, 2018.
- 1252 Yue, D. L., Hu, M., Zhang, R. Y., Wang, Z. B., Zheng, J., Wu, Z. J., Wiedensohler, A., He, L. Y., Huang, X. F.,  
1253 and Zhu, T.: The roles of sulfuric acid in new particle formation and growth in the mega-city of Beijing,  
1254 *Atmos. Chem. Phys.*, 10, 4953–4960, 2010.
- 1255 Zhao, S., Yu, Y., Yin, D., and He, J.: Meteorological dependence of particle number concentrations in an urban  
1256 area of complex terrain, *Atmos. Res.*, 164–165, 304–305, 2015.